AFCRL-64-677

MC 63-80-R1

GAS DYNAMICS OF
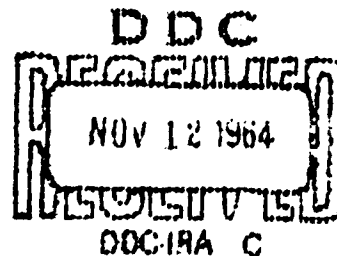HIGH-ALTITUDE ROCKET PLUMES

HENRY L. ALDEN
ROGER H. HABERT

CONTRACT NO. AF19(628)-3280
PROJECT NO. 4984 TASK NO. 498401

FINAL REPORT

JULY 1964

PREPARED FOR
AIR FORCE CAMBRIDGE RESEARCH LABORATORIES
OFFICE OF AEROSPACE RESEARCH
UNITED STATES AIR FORCE
BEDFORD, MASSACHUSETTS

D D C

NOV 12 1964

DDC-IRA C

MITHRAS, INC.

MICROWAVE AND THERMAL RADIATION SENSORS

380 PUTNAM AVENUE, CAMBRIDGE, MASS. 02139

Requests for additional copies by Agencies of the Department
of Defense, their contractors, or other government agencies
should be directed to the

Defense Documentation Center (DDC)
Cameron Station
Alexandria, Virginia 22314

Department of Defense contractors must be established for DDC
services or have their "need-to-know" certified by the cognizant
military agency of their project or contract.

All other persons and organizations should apply to the

U. S. Department of Commerce
Office of Technical Services
Washington, D. C. 20230

MITHRAS, INC.
380 Putnam Avenue
Cambridge, Massachusetts
02139

AFCRL 64-677

MC 63-80-R1

GAS DYNAMICS OF

HIGH-ALTITUDE ROCKET PLUMES

Henry L. Alden
Roger H. Habert

FINAL REPORT

July 1964

Prepared

for

Air Force Cambridge Research Laboratories
Office of Aerospace Research
United States Air Force
Bedford, Massachusetts

FOREWORD

This report was prepared by MITHRAS, Inc., of Cambridge, Massachusetts, for the Upper Atmosphere Physics Laboratory, Air Force Cambridge Research Laboratories, Hanscom Field, Bedford, Massachusetts, under Contract AF19(628)-3280. The work was initiated by Dr. N. W. Rosenberg and monitored by him and Dr. D. Golomb. The research was supported by Advanced Research Projects Agency as part of Project DEFENDER.

The investigations whose results are reported were conducted during the period 1 July 1963 to 30 June 1964. They were directed by Mr. Jacques A. F. Hill and carried out by Mr. Henry L. Alden, and Mr. Roger H. Habert. This final report was written by Mr. Alden.

The work reported here represents a continuation of a program begun during the previous year under Contract AF19(628)-415. This report concludes the work on Contract AF19(628)-3280.

ABSTRACT

This report describes methods for calculation of the velocities and thermodynamic properties of flow fields through and around high altitude rocket plumes. The main effort is directed at obtaining a good representation of both the jet flow from rocket motors and the shock-mixing layers in the frontal regions; the calculation then proceeds downstream using standard methods. The work may be divided in three parts: the development of methods to calculate the flow fields throughout plumes using the principles of inviscid continuum mechanics; the study of the shock-mixing layer structure at the nose of the plume using the general Navier-Stokes equations (i.e., accounting for viscosity, heat conduction and diffusion); and an estimate of validity of continuum mechanics for describing high altitude plumes, as inferred from a study of shock wave formation at high altitudes. A comparison with available observations shows good agreement with overall plume dimensions as determined by the flow-field analysis. It may be concluded that the analysis provides a sound gas-dynamic description which may be used as a basis for investigation of the plasma and chemi-electric properties of high altitude plumes.

MC 63-80-R1

TABLE OF CONTENTS

MC 63-80-R1

LIST OF FIGURES

s

1. INTRODUCTION

As the exhaust gases released by a missile in powered flight expand into the atmosphere, a complex of fluid dynamic, chemical and radiative phenomena occur. These are associated with a large visible plume which forms around the rocket and trails behind it, as shown by Rosenberg (1961). The radiative phenomena are "observables" and have been subjected to the most intensive observation. In order to understand how they arise and what form they may take in new situations, it is necessary to study the chemistry, plasma properties and fluid dynamics of the plumes.

The work reported here is concerned with the fluid dynamic aspects of missile trails, and especially with the motions of both the air and rocket gases which create the plumes. It is thus an extension of early work by Hill and Habert (1963). In the latter a simple theory was developed for the size and shape of high altitude plumes, and the dependence of these properties on altitude, motor size, nozzle geometry, combustion pressure and forward speed. The general plume was described by a two-parameter family of ellipsoids; using a simple blast wave theory the radius of curvature at the nose was evaluated, while the plume length was calculated using the concept of plume drag. Comparison between predictions and optical observations showed excellent agreement in nose radii and maximum diameters. In addition it was shown that it is reasonable to use the methods of continuum mechanics to study the flows in plumes. An appropriate approximation to the Navier-Stokes equations was developed for the structure of the mixing layer in the frontal regions, where it is merged with both the external and internal shock waves. The success of the early work suggested that it would be possible to develop methods to evaluate the entire flow field in plumes, a goal of great practical interest since it would permit calculation of air-gas densities, chemical reactions and electro-optical properties.

This report describes the application of theoretical principles to the problem of devising methods to calculate the velocities and thermodynamic properties of flow fields through and around high-altitude plumes. The main effort is directed at obtaining a good representation of both the jet flow from rocket motors and the shock-mixing layers in the frontal regions. Farther downstream, and at larger distances laterally from the plume axis, standard methods are available. The work may be divided in three parts: the development of methods to calculate the flow fields throughout plumes using the principles of inviscid continuum mechanics; the study of the shock-mixing layer structure at the nose of the plume using the general Navier-Stokes equations (i.e. accounting for viscosity, heat conduction, diffusion); and an estimate of the validity of continuum mechanics for describing high

MC 63-80-R1

altitude plumes, as inferred from a study of shock wave formation at high altitudes.

It should be noted that in this work there is the requirement that the gross properties of plumes, such as nose radius and length, be predictable from the detailed flow picture, and that they must agree with the simple methods already developed in the early work, as well as with observation of flights.

MC 63-80-R1

2. SUMMARY AND CONCLUSIONS

Methods have been developed to calculate flow fields in rocket plumes at high altitude. These, together with the technique of Witham (1960) supply a complete and practical way to analyze the field properties (velocities and thermo-dynamic quantities) using the principles of inviscid continuum mechanics. The methods may be described as follows.

a. The inner flow from the rocket nozzle is identical to that which would occur in a vacuum. The inviscid, perfect-fluid formulation of gas dynamics is used to obtain asymptotic equations for continuous flows issuing from nozzles into a vacuum. A method of series expansion is employed such that the first term represents the final (limiting) flow at very large distances from the nozzle. The general solution for higher order terms is demonstrated. Specific solutions for first and second order terms are obtained. The flow is described as a series of perturbations of a flow everywhere radial and at the limiting velocity; the angular distribution of mass flux along various radial directions, according to the theory, can be chosen arbitrarily and can therefore be used to match the initial conditions of the flow near the nozzle. The latter conditions must be obtained independently by experiment or calculation, e. g., by the method of characteristics.

b. The surface of the plume is conveniently described, in the inviscid approximation, by the dividing streamline separating the outer air flow from the inner flow of rocket gases. Starting with the approximations of hypersonic flows, the inviscid plume equation is set up which, when integrated, locates the surface of dividing streamlines. The equation is integrated for representative cases.

c. With the dividing streamlines as reference, the location and properties of the double shock layer are expressed algebraically.

d. Flow directly downstream of the rocket is returned to atmospheric pressure through a mach disc which is located by the methods of Hill and Habert (1963); flow outside the wake of rocket gases and behind the frontal regions of the plume can be analyzed by the technique of Witham. Thus the set of methods (a)-(d) is a complete system for inviscid plume analysis,

3   MC 63-80-R1

The flow at the nose of plumes has been analyzed using the Navier-Stokes equations accounting for viscosity, diffusion and heat conduction. The reduced equations of Hill and Habert (1963) were integrated using the method of influence coefficients to satisfy the split boundary conditions. This method gave a set of numerical results for the flow pattern in the merged layer around a spherical release; the analysis represents the first computation of its kind. It was found however that the method was inherently awkward and slow. To remedy this a second method was developed for programming in FORTRAN. The problem is one of integrating a set of eight first-order ordinary differential equations which are restricted by a set of split boundary conditions. Development of the new method was accomplished through the use of a set of asymptotic (analytic) solutions to the equations, an approach which greatly simplifies the numerical program.

The numerical results from the first method show the structure of the merged layer for one particular flight condition, and demonstrate the adequacy of the basic formulation of the problem to represent the variation o properties in the merged layer.

The study of shock wave formation at high altitude shows that no completely satisfactory criterion for shock wave formation has yet been established in the field of rarefied gas-dynamics. A plausible criterion can be developed however, expressible in terms of the ratio of shock thickness to plume (or body) radius. Application of this criterion to rocket plumes leads to the result that typical ICBMS and IRBMS will generate a bow shock all the way to burnout of the last stage (SECO).

4

3. INVISCID PLUME FLOW

3.1 General

The plume shape behind a rocket is the result of interaction between the atmosphere, the forward motion of the missile, and the jet flow from the rocket motor. The inviscid flow model is that shown in Fig. 3.1. The coordinate axes are fixed in the missile, thus giving the atmospheric free stream a velocity relative to the origin. Behind the rocket is a region in which the flow is identical to the flow of a jet exhausting to vacuum. This region is bounded by an inner shock which alters the jet velocity and pressure to accommodate them to the oncoming free stream. The latter must also accommodate itself by passing through an outer shock. In between the two shocks is a zone called the merged layer in which the two gases flow together downstream. In reality the gases mix, and the shocks extend well into the layer because of viscous forces. The properties of the layer are complex and depend on the effects of viscosity, diffusion, heat transfer and the properties of real gases. A discussion and analysis of these complications are taken up in a separate section (4). In the idealized inviscid model the layer can be thought of as flowing in two parallel sublayers of unmixed gases, separated by a contact surface as indicated by the dotted line in Fig. 3.1. Directly downstream from the rocket, the region of jet flow is returned to atmospheric pressure by a combination of shock and viscous processes which are not yet known. For this model it will suffice to assume that the jet flow is returned to ambient pressure through a normal shock in the rear. This condition determines the location of the rear shock and the flow behind it for the inviscid model.

In order to analyze the inviscid plume model it is first necessary to have a knowledge of the jet flow from the rocket motor at large distances from the nozzle exit. To this end a general analysis was made of asymptotic flows of jets exhausting a vacua. The results provide a method of representing the asymptotic flow behind any rocket motor in a useful form. With this as a basis, the analysis of rocket plumes was then carried out to obtain the shape and position of the contact surface in the merged layer.

In Section 3 an account is given of the development of general formulas for the asymptotic flows of jets. This is followed by a description of the inviscid plume equations and their solution in certain cases. These results are then examined in the light of experimental data. Finally a discussion is given of the next steps in the analysis of the rocket plume problem.

MC 63-80-R1

6

REGION COMPOSED OF
OUTER SHOCK, CONTACT
SURFACE AND INNER
SHOCK

ROCKET

M_∞

EXTERIOR
BOW SHOCK

CONTACT SURFACE

INNER SHOCK

JET FLOW
REGION

MACH DISK
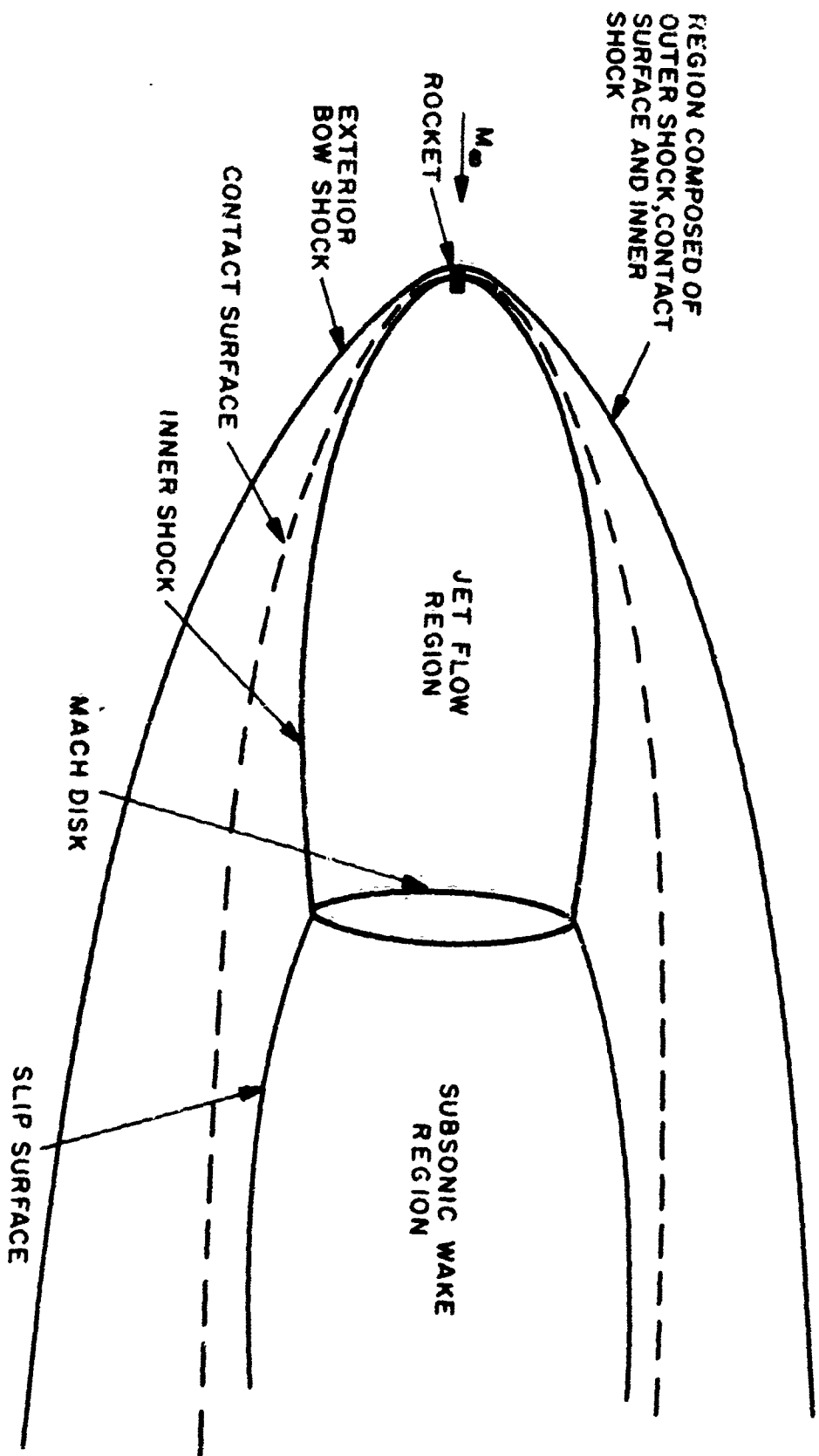
SUBSONIC WAKE
REGION

SLIP SURFACE

Figure 3.1. Inviscid Flow Model of High Altitude Plumes

3.2 The Asymptotic Flows of Jets Exhausting into Vacua

There exist simplified representations of flows from jets, such as that of Mirels and Mullen (1962) using the concept of hypersonic similitude, and that of the Convair/Astro group, using the concept of simple source flow. These methods aim at representing the flow of jets at large distances from the nozzle. There are other methods which deal with the flow close to the nozzle, notably the method of characteristics as employed by Bowyer (1958). There is a large region of the flow, however, which is intermediate between these two zones of application, and in which either method presents difficulties. To carry the method of characteristics downstream for thousands of nozzle diameters is impractical. To employ the source flow concept properly requires that this flow be matched to the initial flow conditions close to the nozzle, but this region is just where the simple source concept is not valid. The same is true of the hypersonic similarity method. For these reasons a new approach has been taken in which the rigorous non-viscous equations of motion are solved by using an asymptotic series expansion in terms of reciprocal powers of r, the radial distance downstream measured from the nozzle. The first two terms of this expansion are equivalent to the source-flow concept of Mirels and Mullen (1962); higher terms in the series permit the flow to be matched to the flow close to the nozzle, and give a sound estimate of the errors involved in dropping higher order terms from the calculations. A brief account of the method is given in the paragraphs below, while a more detailed description is given in MITHRAS report No. 376A.

The basic equations for inviscid compressible flows are developed by Tsien (1958). The natural coordinate system for this investigation is spherical, with the origin located at the rocket nozzle and the x_3 axis directed downstream along the nozzle axis (see Fig. 3.2). The flow is rotationally symmetric around the x_3 axis, and has a velocity u along the radius r and a velocity v at right angles to r. The equations of continuity and irrotationality take the following form in any plane $\omega = $ const:

$$\left\{ a^2 - u^2 \right\} \frac{\partial u}{\partial r} - uv \left\{ \frac{\partial v}{\partial r} + \frac{1}{r} \frac{\partial u}{\partial \theta} \right\} + \left\{ a^2 - v^2 \right\} \frac{1}{r} \frac{\partial v}{\partial \theta}$$

$$= - \frac{a^2}{r} \left\{ 2 u + v \cot \theta \right\} \tag{3.1a}$$

$$\frac{\partial v}{\partial r} - \frac{1}{r} \frac{\partial u}{\partial \theta} + \frac{v}{r} = 0 \tag{3.1b}$$

u = radial velocity

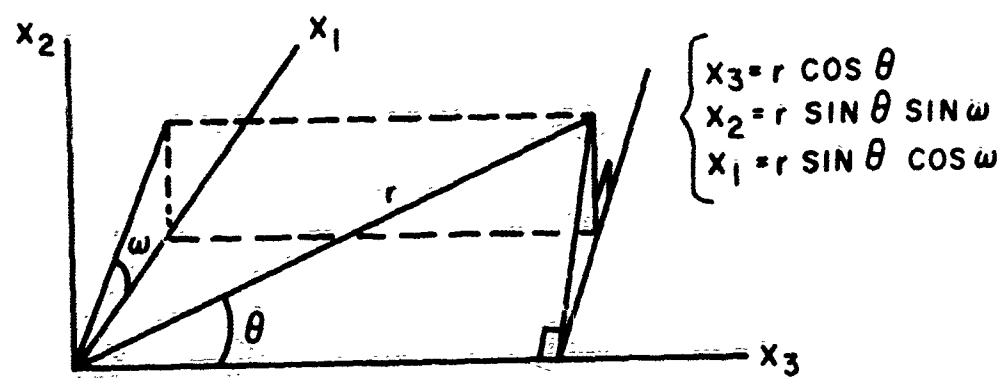v = angular velocity

a = local sonic velocity

MC 63-80-R1

Figure 3.2. Coordinate System for Jet Flow

The equations of motion can be integrated independently of (3.1) to give a relation between the magnitude of the velocity and the thermodynamic properties of the flow:

$$a^2 = \frac{\gamma - 1}{2} \; c^2 \left[1 - (U/c)^2 \right] \tag{3.2}$$

$$U^2 = u^2 + v^2$$

γ = ratio of specific heats

c = limiting velocity of flow

Equations (3.1a) and (3.1b) are homogeneous in dimensional velocities as well as r, and may be normalized by dividing by $c^3 y^*$, where y^* is a reference length which will be taken to be the throat radius of the rocket nozzle. All velocities can be replaced by (u/c), (v/c), and r by r/y^*; this substitution will be assumed in what follows. The solution of (3.1) by asymptotic expansion is carried out by expressing (u/c) and (v/c) in the form of appropriate series. These are:

$$\frac{u}{c} = \sum_{n=0}^{\infty} c_n f_n (\theta) \; r^{-2n (\gamma - 1)} \qquad f_0 (\theta) = 1$$

$$f'_0 (\theta) = 0$$

$$\frac{v}{c} = \sum_{n=0}^{\infty} f'_n (\theta) \; r^{-2n (\gamma - 1)} \qquad c_n = \left[1 - 2n (\gamma - 1) \right]$$

$$(') = d/d\theta \tag{3.3}$$

The form of v/c is not independent, but is picked so that, together with u/c, it satisfies (3.1b). The series (3) are now substituted in (3.1a) to obtain the equations for the f_n which result from setting the coefficient of each power of r equal to zero. The terms with a^2 require the use of (3.2). The result of these substitutions is to show that $f_1 (\theta)$ can be an arbitrary function of θ while the higher order f_n are algebraic functions of $f_1 (\theta)$ and its derivatives.

The thermodynamic properties can be expressed in terms of the solution (3.3) by using the standard relationships of isentropic flows. Pressure, density, and temperature in the jet flows are given to the first order by:

$$p/p_o = \frac{\left\{ 2(3-2\gamma)(-f_1)\right\}^{\frac{\gamma}{\gamma-1}}}{r^{2\gamma}}$$

$$\rho/\rho_o = \frac{\left\{ 2(3-2\gamma)(-f_1)\right\}^{\frac{1}{\gamma-1}}}{r^2} \qquad\qquad (3.6)$$

$$T/T_o = \frac{2(3-2\gamma)(-f_1)}{r^{2(\gamma-1)}}$$

To investigate the matching of asymptotic flows to near-nozzle flows, it is necessary to express some properties of the flow to higher orders than the first. A convenient property for this purpose is the reciprocal of the square of the Mach number, a^2/U^2. It contains in the first term the function $f_1(\theta)$ as a linear factor. The near nozzle calculations of Bowyer (1958) give (U/a) explicitly and thus provide a simple way to determine the form of $f_1(\theta)$. The formula for $a^2/U^2 = (1/M^2)$ is, including the second order term:

$$\frac{1}{M^2} = \frac{(\gamma-1)(3-2\gamma)(-f_1)}{r^{2(\gamma-1)}}$$

$$+ \left\{ 3(3-2\gamma)^2 f_1^2 - 2(5-4\gamma)f_2 - f'^2_1 \right\} \cdot \frac{(\gamma-1)}{2r^{\frac{4(\gamma-1)}{}}} \cdots$$

$$(3.7)$$

where

$$2(5-4\gamma)f_2 =$$

$$\overline{A}\, f_1^2 + \overline{B}\, f_1 f'_1 \cot\theta + \overline{C}\, f'^2_1 + \overline{D}\, f_1 f''_1$$

and

$$\overline{A} = -(3 - 2\gamma)^2 (2\gamma - 1)$$

$$\overline{B} = (3 - 2\gamma)$$

$$\overline{C} = \frac{4 - 3\gamma}{\gamma - 1}$$

$$\overline{D} = (3 - 2\gamma)$$

To match flows it is first necessary to choose a suitable form for $f_1(\theta)$. This is most easily explained by reference to the sketch of Fig. 3.3. The flow emerges from the nozzle at the left under known conditions of Mach number and angular distribution. The flow expands to some maximum angle θ_M, and distributes itself in a fan-shaped pattern of streamlines which eventually become radial. The pattern near the nozzle is that calculated by Bowyer (1958); it is straightforward to read off values of Mach number and compute $1/M^2$ for varying θ at constant radii for comparison with (3.7). For a particular nozzle a plot of these points for r = 60 is shown on Fig. 3.4 (normalized to 1.0 at $\theta = 0$). From (3.7) it is seen that in the first approximation this curve is the function $f_1(\theta)$. The near nozzle computations thus indicate the general form of $f_1(\theta)$. They suggest several possible curve fits. It will be expedient to choose the representation

$$f_1(\theta) = \frac{\lambda}{(3 - 2\gamma)} \left\{ \frac{\cos\theta - \cos\theta_M}{1 - \cos\theta_M} \right\}^{4(\gamma - 1)} \qquad (3.8)$$

θ_M = effective maximum expansion angle

λ = normalizing constant

$$\frac{\lambda}{(3 - 2\gamma)} = \frac{-1}{(\gamma + 1)} \left[\left(\frac{\gamma - 1}{\gamma + 1} \right)^{\frac{1}{2}} \frac{5}{2(1 - \cos\theta_M)} \right]^{\gamma - 1}$$
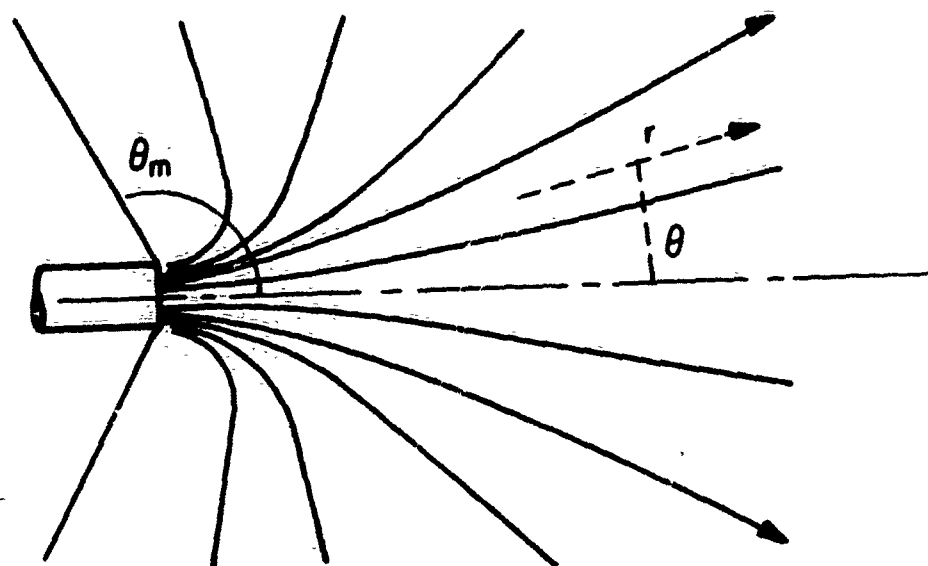
Figure 3.3. Jet Streamlines

MC 63-80-R1

This curve fitting function is shown on Fig. 3.4. The particular form chosen here lends itself to easy computation in the applications that follow.

Having picked a suitable form for $f_1(\theta)$, one can now match flows. For this the nozzle is that of Figs. 4, 5, and 7 of Bowyer (1958). The flow emerges with a semi-divergence angle of 15°, a nominal exit Mach number of 2.843, a nominal area ratio (exit to throat) of 5:1, and a γ of 1.225. If the asymptotic series is a correct representation, then the matching problem reduces to the proper selection of two parameters: y^*, the throat radius; and the nominal angle of maximum expansion, θ_M. The first matching is done along the flow axis ($\theta = 0$) to obtain an effective value of y^*. For this, formula (3.7) can be reduced to

$$\left(\frac{1}{M^2}\right)_{\theta\,=\,0} =$$

$$\frac{(\gamma - 1)(-\lambda)}{r^{2(\gamma-1)}}\left[1 + \left\{2(\gamma + 1) + \frac{8(\gamma-1)}{(3-2\gamma)(1-\cos\theta_M)}\right\}\cdot\right.$$

$$\left.\cdot\frac{(-\lambda)}{2r^{2(\gamma-1)}}\cdots\right] \tag{3.9}$$

Although this formula is dependent on θ_M, it is not sharply sensitive to it; a value of θ_M can be picked based on maximum Prandtl Meyer expansion angles, and then adjusted later without upsetting the first calculations.

The value of y^* is at first taken to be the nominal value, and then adjusted slightly to obtain a curve fit at large r. The result of this process is shown in Fig. 3.5, in which the solid line is 3.9 and the dotted line is the first term (the so-called linear solution). It is seen that the second order solution tends toward the linear as r gets large, but that convergence is not rapid. The exact calculations are taken from Bowyer (1958) and are shown as the encircled points. To obtain a fit, a value of y^* was picked such that y^* equalled y_e, the exit radius, divided by 2.22; the nominal factor is $\sqrt{5} = 2.24$. This result promotes confidence that the 2nd order solution is adequate to match flows near the nozzle, and that the first order solution is quite accurate for r > 500. Below a value of r = 7, exact flow deviates sharply from the asymptotic; this point corresponds to the arrival at the center line of the Mach wave from the lip of the nozzle. It is to be expected that such deviations would occur since the asymptotic flows are assumed to issue from a point. It should also be noted that the point of origin for measuring r is displaced downstream from the nozzle. The origin is found by passing a line through the nozzle lip at an angle of θ_M and locating r = 0 where this line crosses the nozzle axis.
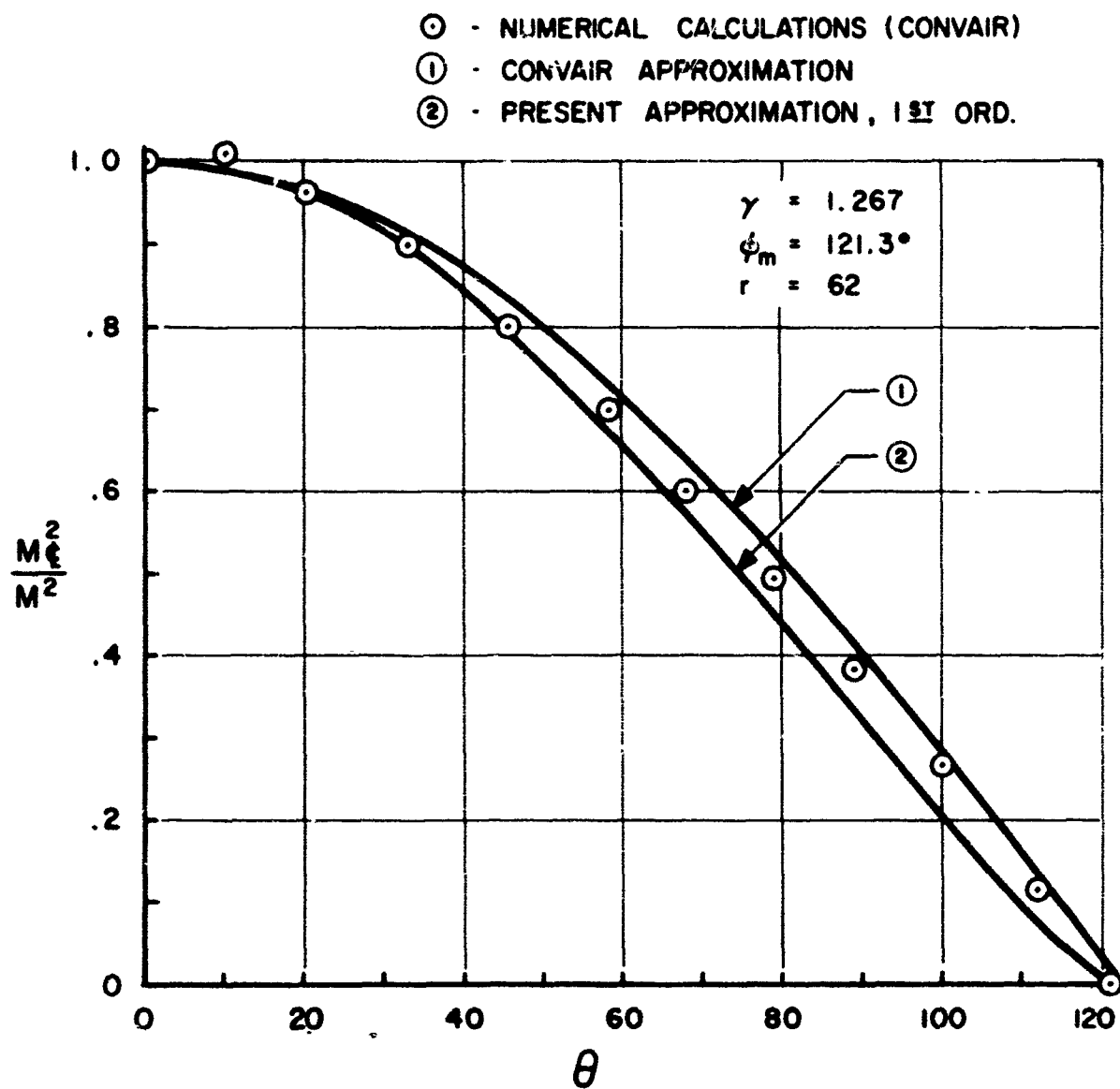
13 MC 63-80-R1

Figure 3.4. Asymptotic Jet Expansion Theory Matching Flows with Near- Nozzle Calculations.
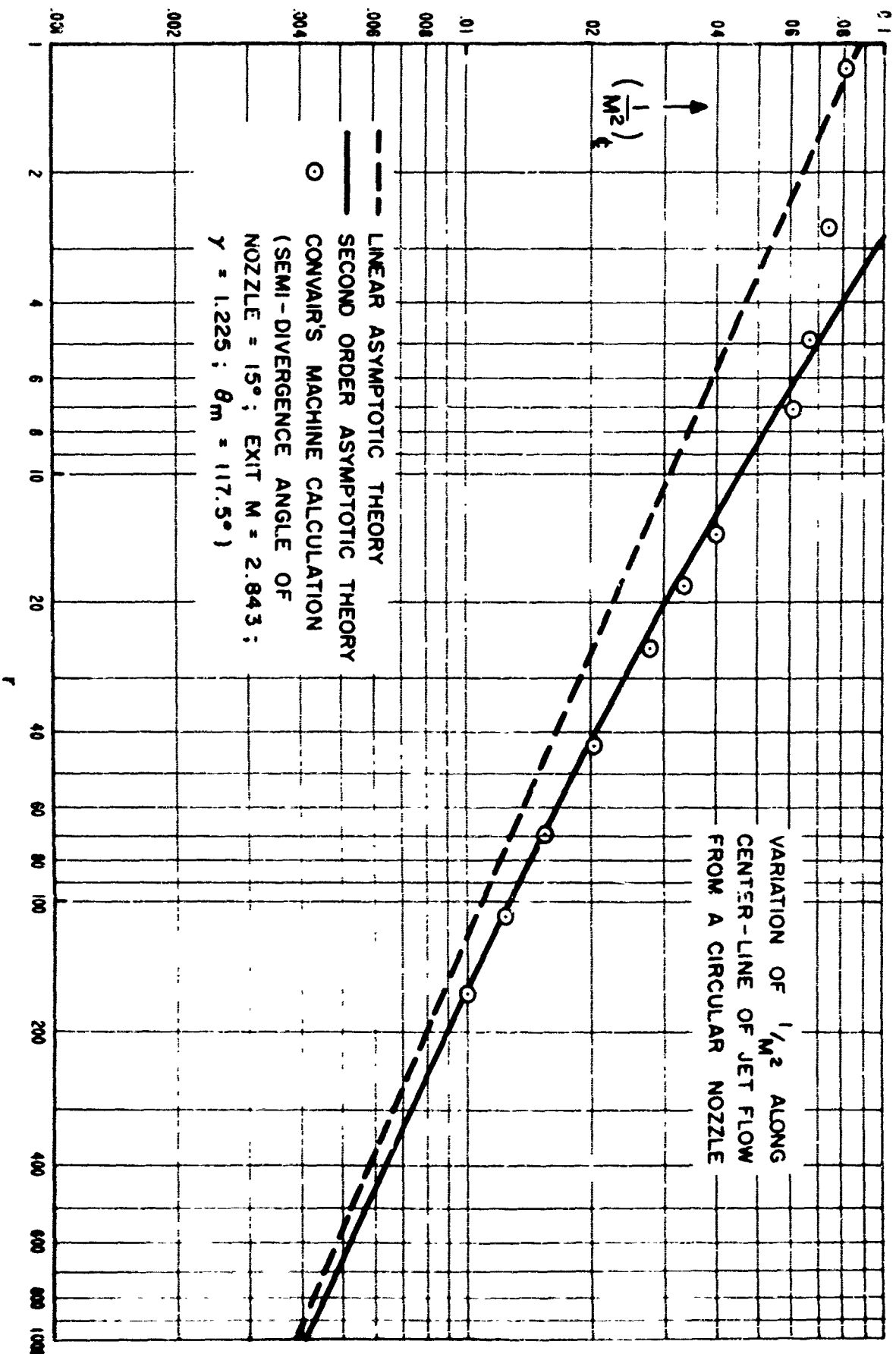
14 MC 63-80-R1

Figure 3.5. Asymptotic Jet Expansion Compared with Convair's Machine Calculations.

The next step is to select an effective value of θ_M. This is done by examining the function $(1/M^2)$ at r = constant and picking θM to obtain the best fit for the variation of $(1/M^2)$ with θ. The adequacy of this procedure can then be checked by comparing the flows at other values of r. In the example here the near-nozzle data for r = 130 were used and θ_M picked to be 117.5^O. The variation of $1/M^2$ with θ at r = 139 is shown on Fig. 3.6, together with the rigorous near-nozzle calculation. As a check, a similar comparison is plotted for r = 42. It appears that the agreement is good, and that the small changes observed are adequately represented by the second order theory. The linear solution, representing the flow as $r \rightarrow \infty$, is shown on Fig 3.6 as the dotted line. It should be noted that the curves are normalized to equal unity at θ = 0; compared to the values at the axis, then, the second order effect is to reduce $(M)^2_{\theta = 0} /M^2$ below its final (linear) value. However, by referring to Fig. 3.5, it is seen that the second order effect is to increase the values of $(1/M^2)$ over the linear values on the axis. The two effects tend to cancel in the off-axis regions. Thus it can be said in the present examples that the linear solution approximates the exact solution to 10 percent or better for r = 500, and θ ranging between $\pm 100^O$, and that any error will become a successively smaller percent as r increases.

The result of the investigation of this section is a set of asymptotic formulas which give all flow properties of jets in the regions of "intermediate" flow and far downstream of nozzle exits. The method provides estimates of errors. The validity and accuracy of the linearized asymptotic formulas are established. The pertinent formulas are (3.3) for velocities, (3.8) for flow distribution and (3.6) for thermodynamic properties.

In concluding this section, three properties of jet flows are developed which will be needed in later calculation of plume dynamics. These are the mass flow, total pressure force and the total momentum of jet flow across downstream boundaries. The boundaries in question are spherical (at constant r) and bounded by circles of constant θ; an example is the right-hand boundary of Fig. 3.8 . The horizontal force at the boundary arising from pressure is given by

$$F_j = 2 \pi r \int_o^\theta \cos\theta \cdot p_j \cdot dy$$

$$= 2 \pi r^2 \int_o^\theta \sin\theta \cos\theta \cdot p_j \, d\theta \quad , \quad p_j \text{ from eq. 3.6}$$

$$= \frac{\dot{m}_j c_j \, g\,(\gamma_j)}{r^{2(\gamma-1)}} \cdot h\,(\theta; \theta_M, \gamma_j) \tag{3.10}$$

g, h are the functions. $\dot{m}_j$ is the total mass flow of the jet and c_j its limiting velocity.
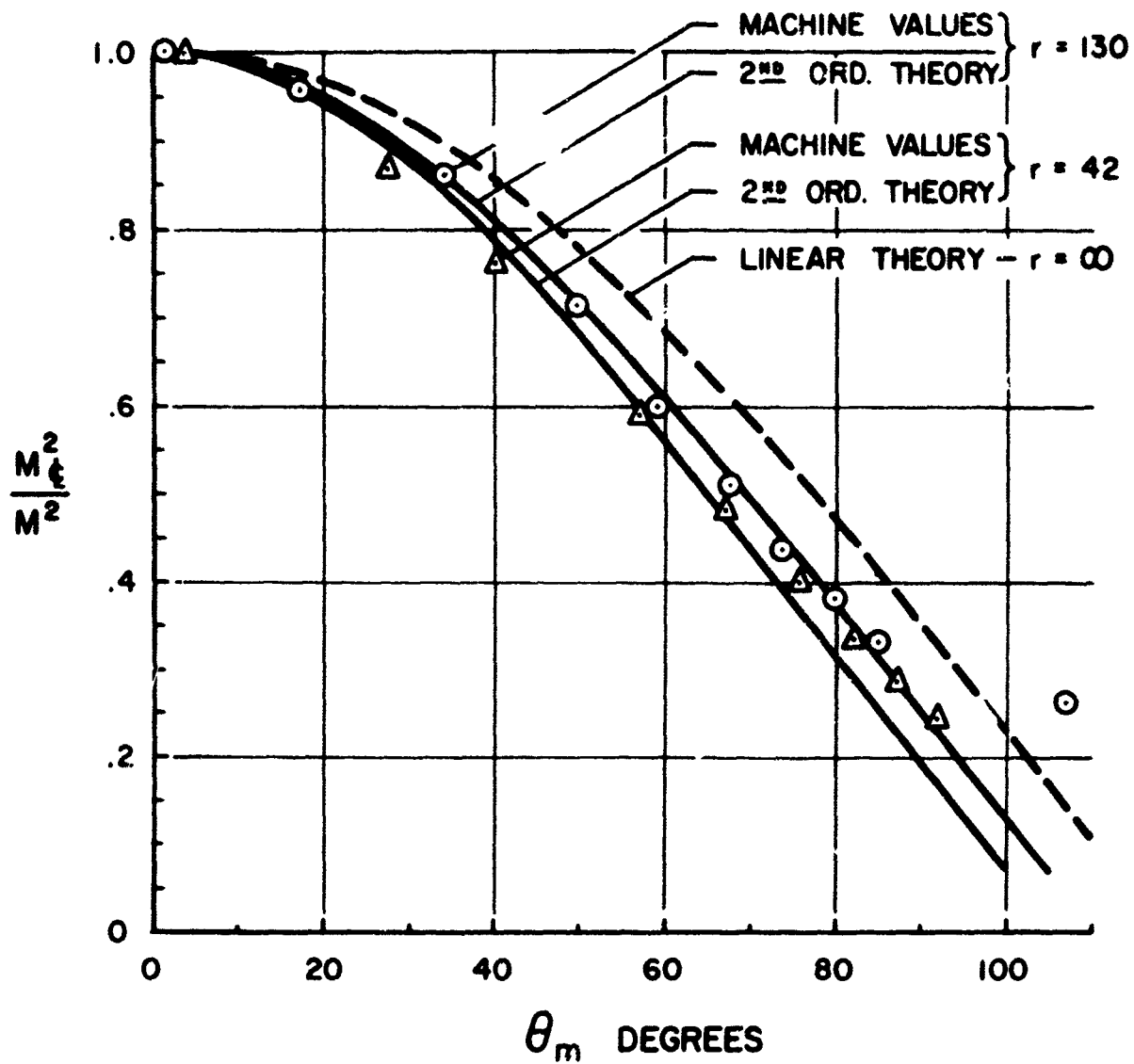
16   MC 63-80-R1

Figure 3. 6 Asymptotic Jet Expansion Comparison with Machine Calculations $\gamma = 1.225$, $\theta_m = 117.5^{\circ}$

The form of h and g are easily determined; the main result needed here however is that F_j has no zero order term, but goes to zero with r as $(1/r)^{2(\gamma-1)}$. It is understood that this is the first term of an asymptotic series, just as are equations 3.6.

The second property of interest is the integrated mass flow across the same boundary. In the first approximation it is

$$\dot{m}_j(\theta) = 2\pi r^2 \int_0^\theta \rho_j u_j \sin\theta \, d\theta$$

$$= 2\dot{m}_j \, (\frac{\rho_c}{\rho^*}) \, (\frac{c_j}{a^*}) \int_0^\theta (-2\lambda f_1)^{\frac{1}{\gamma_j - 1}} \sin\theta \, d\theta$$

$$= \dot{m}_j \left\{ 1 - \left(\frac{\cos\theta - \cos\theta_M}{1 - \cos\theta_M}\right)^5 \right\} \tag{3.11}$$

The mass flow between θ_M and θ through a spherical ring would hence be $\dot{m}_j - \dot{m}_j(\theta)$; expression 3.11 is the first (zero order) term of an asymptotic expansion.

Finally the integrated momentum across the boundary between 0 and θ may be computed as

$$\dot{M}_j(\theta) = \int_0^\theta \left\{ d\dot{m}_j(\theta)/d\theta \right\} c_j \cos\theta \, d\theta \tag{3.12}$$

$$= \dot{m}_j c_j \left[1 - g^5(\theta) \cdot \cos\theta + (\frac{1 - \cos\theta_M}{6})(g^6(\theta) - 1) \right]$$

where

$$g(\theta) = \frac{\cos\theta - \cos\theta_M}{1 - \cos\theta_M}$$

3.3 The Inviscid Plume Equations

The photographic evidence of Rosenberg (1961) shows the plume to be roughly parabolic at the head, tapering downstream to a wake having a maximum width. Since the forward speed of the missile is highly supersonic, the flow field around the plume is hypersonic, at least as far back as the region where the hypersonic parameter $(M^o \sigma^o)$ is of the order (1). Here M^o is the free stream Mach number, and σ^o is the local slope of the plume surface in radians. For a typical forward speed of $M^o = 7$, $\sigma^o \approx 8^o$; this means that the greater part of the head of the plume is subject to hypersonic flow conditions; this fact will be assumed in the initial analysis. For the purpose of setting up force and momentum balances the division between the outer flow of

the free stream and the inner jet flow will be assumed to be a surface located approximately at the contact surface shown in Fig. 3.1. The first step is to set up a force-momentum balance which will determine the location of this surface. Following this, more detailed considerations will position the inner and outer shocks and fix conditions in the merged layer. A force-momentum balance normal to the plume surface will consist of three parts:

(a) the hypersonic pressure reaction as the freestream enters the merged layer;

(b) the hypersonic pressure reaction of the jet flow as it enters the same layer from the inside; and,

(c) the centrifugal pressure of the mass flow in the merged layer.

The pressures (a) and (b) will be termed p_{ML}^o and $p_{ML, j}$, respectively. The centrifugal pressure (c) can be obtained from the centrifugal force (outward) per unit arc length along the plume, designated $\Delta F/\Delta S$; this is the force which would be exerted on a strip of length $2\pi r \sin\theta$ and of unit width, assuming the strip was straight so that the pressure forces were additive. The coordinate system is sketched in Fig. 3.7, and is taken to be consistent with that of the previous section. The normal force balance states that (a) equals the sum of (b) + (c) at every point, or

$$p^o_{ML} = p_{ML, j} + \frac{\Delta F}{\Delta S} \cdot \frac{1}{2\pi r \sin\theta} \qquad (3.13)$$

The pressures are given by the hypersonic formulas:

$$p_{ML} = \gamma^o p^o M^{o2} \sin^2 \sigma^o$$

$$p_{ML, j} = \gamma_j p_j M_j^2 \sin^2 \sigma_j \qquad (3.14)$$

$(\ )^o$ = free stream conditions

$(\ )_j$ = jet conditions

for σ^o, σ_j, see Fig. 3.7

It is straightforward to show that

$$\frac{\Delta F}{\Delta S} = \frac{\dot{m}_{ML} V_{ML}}{R} \qquad (3.15)$$

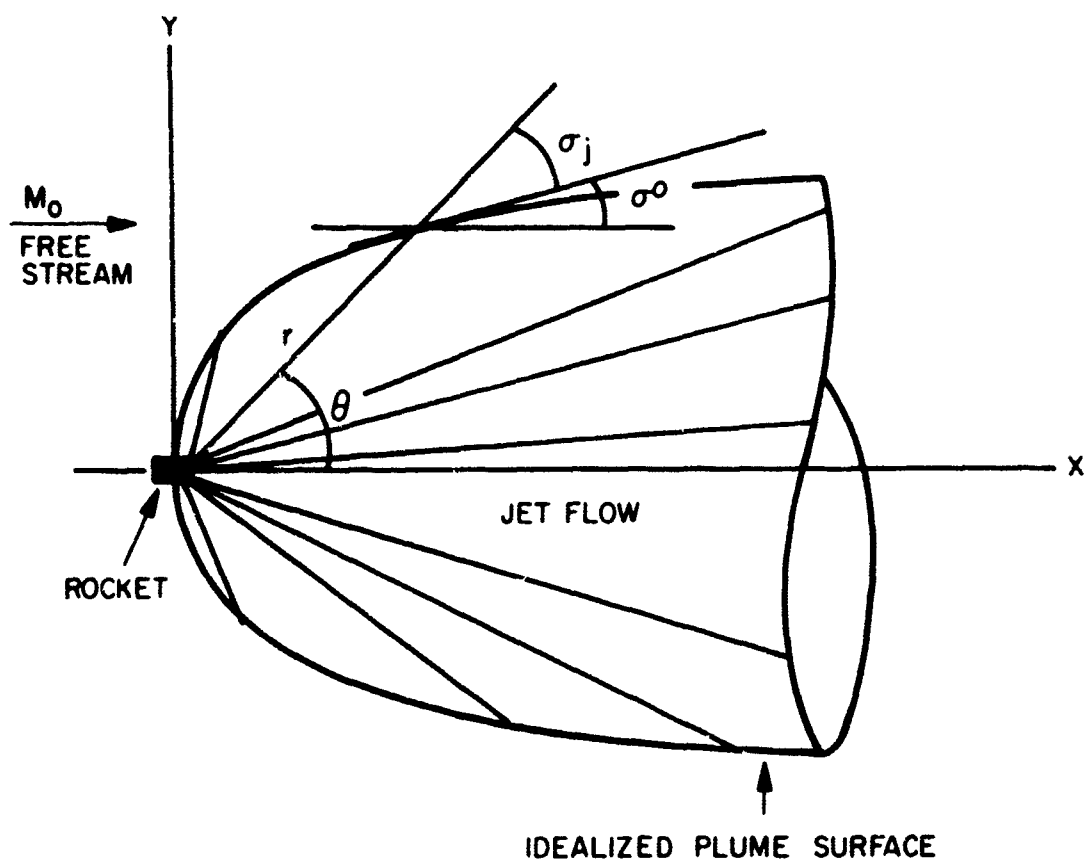Figure 3. 7. Coordinates for Calculation of Idealized Plume Surface

MC 63-80-R1

where

$$\dot{m}_{ML} = \text{mass flow in the merged layer}$$

$$V_{ML} = \text{average velocity of the merged layer}$$

$$R = \text{radius of curvature (+) of the plume surface in the } (r, \theta) \text{ plane}$$

Putting (3.14) and (3.15) in (3.13, and normalizing by dividing by p_c (the chamber pressure of the rocket motor), one gets

$$\frac{2q^o}{p_c} \sin^2 \sigma^o = \gamma_j \left(\frac{p_j}{p_c} \right) M_j^2 \sin^2 \sigma_j$$

$$+ \frac{\dot{m}_{ML} V_{ML}}{p_c y^{*2}} \cdot \frac{1}{2\pi r \sin\theta} \cdot \frac{1}{R} \qquad (3.16)$$

where both r and R have been non-dimensionalized by y^*.

and

$$q^0 = \text{free stream dynamic pressure}$$

$$\theta = \sigma^o + \sigma_j \quad (\text{see Fig. 3.7})$$

$$\frac{1}{r} \frac{dr}{d\theta} = -\cot \sigma_j \qquad (3.17)$$

Equation (3.16) gives the inviscid plume surface. It is a second order differential equation for the spherical radius r as a function of θ. The second term on the right accounts for the centrifugal pressure, and adds considerable complexity to the equation. The second derivative appears in R, the radius of curvature; furthermore the factor $\dot{m}_{ML}$ times V_{ML} is not constant, and must be obtained from an independent relation. In the course of solving the equation a simplified relation was first used, obtained from (3.16) by dropping the centrifugal term. The results of solving this equation did not show a close correspondence with the data. Also it is possible to show that the centrifugal term should be retained on the basis of an order of magnitude analysis. The solution given here consequently will be for the full second order relation (3.16).

The solution of (3.16) requires expressions for $(p_j/p_c) M_j^2$ and $(\dot{m}_{ML} V_{ML})$. The first is obtained from the jet flow functions of the previous section (using only the linear approximation as given in eqa. 3.6 and 3.7). To obtain an expression for the variation of $(\dot{m}_{ML} V_{ML})$

one can set up an integral force-momentum balance in the axial direction. The control volume in which the balance is to be computed is shown in Fig. 3.8. The "ingoing" quantities are free stream pressure and momentum over an area of $\pi r^2 \sin^2\theta$, and the motor pressure and momentum. These are balanced by the outgoing momentum of the merged layer, the outgoing momentum of the jet flow from the right hand boundary and the jet flow pressure over the same boundary. The ingoing quantities are

$$\pi r^2 \sin^2\theta\,(p^o + \rho^o U^2) + \pi y_{ex}^2\,(p_{ex} + \rho_{ex} U_{ex}^2)$$

$$\cong \pi y*^2 p_c \left[2(\sqrt{q^o/p_c}\,r)^2 \sin^2\theta + C_F^o\right] \tag{3.18}$$

where

$$q^o = \frac{\gamma^o}{2}\,p^o M^{o2} = \text{free stream dynamic pressure}$$

$$C_F^o = \text{vacuum thrust coefficient}$$

$$= \frac{\text{Vacuum Thrust}}{\pi p_c y*^2} \quad \text{(definition)}$$

$$= \frac{(p_{ex} + \rho_{ex} U_{ex}^2)}{p_c}$$

$(\ )_{ex}$ indicates conditions at rocket motor exit.

The approximation made in (3.18) is that p^o/q^o is small, i.e., the same as that made in the hypersonic formulas (3.14). The outgoing quantities are

$$\left[\dot{m}_{ML} V_{ML} \cos\sigma^o + \dot{M}_j(\theta) + F_j\right]$$

$\dot{m}_{ML} V_{ML} \cos\sigma^o$ = outgoing momentum of the merged layer

$\dot{M}_j(\theta)$ = outgoing momentum of the jet flow across the right boundary of Fig. 3.12 which can be obtained from the asymptotic jet formulas (See Eq. 3.12).

V_{ML} = average velocity of merged layer.

$\dot{m}_{ML}$ = average mass flow in merged layer.

$\dot{m}_j$ is mass flow of rocket motor and is constant; $\dot{m}_{ML}$ varies with location along the merged layer.

F_j = pressure force of jet at right boundary; it can be obtained from the asymptotic formulas of (3); it is to the lowest order term (see Eq. 3.10):
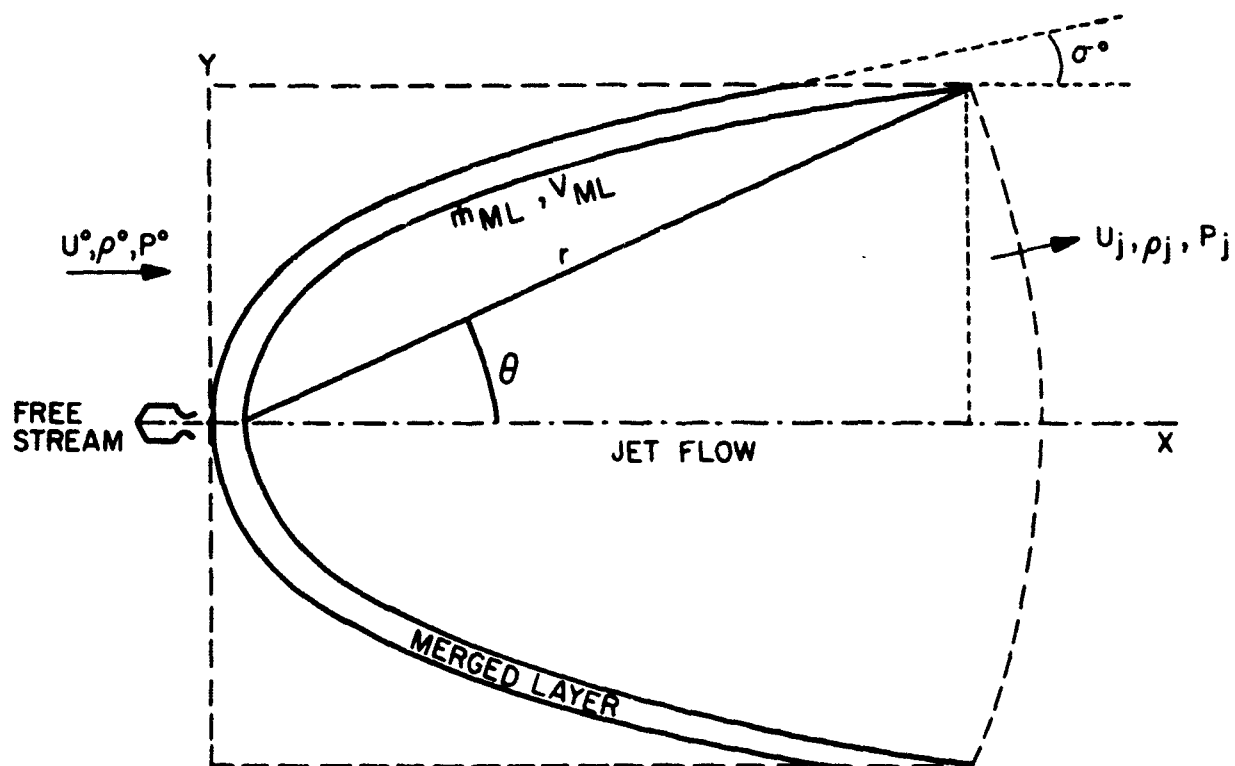
Figure 3. 8. Control Volume Geometry for Horizontal For.e
Balance

$$= \frac{\dot{m}_j c_j g(\gamma_j)}{r^{2(\gamma_j - 1)}} \left[h(\theta; \theta_M, \gamma_j) \right]$$

The expressions for $\dot{M}_j(\theta)$ and F_j are the first terms in the asymptotic series in $1/r^{2n(\gamma_j - 1)}$. $\dot{M}_j(\theta)$ starts with a zero order term, and F_j with one of first order, which may be dropped by comparison in the approximation here. The horizontal force balance can now be written as

$$\pi y*^2 \, p_c \left[2 \, (\sqrt{q^o/p_c} \; r)^2 \, \sin^2\theta + C_F^o \right]$$

$$= (\dot{m}_{ML} V_{ML}) \cos\sigma^o + \dot{M}_j(\theta)$$

and

$$C_F^o = \dot{M}_j(\theta_M)/\pi y*^2 p_c$$

The expression $(\dot{m}_{ML} V_{ML})$ can now be put in terms of r, θ, and σ^o:

$$\frac{\dot{m}_{ML} V_{ML}}{\pi y*^2 p_c} = \frac{1}{\cos\sigma^o} \left[2\bar{r}^2 \sin^2\theta + \mu(\gamma_j)g^5 \left(\frac{5\cos\theta + \cos\theta_M}{6} \right) \right] \tag{3.19}$$

where

$$\bar{r} = \sqrt{q^o/p_c} \cdot (r/y*); \; \mu(\gamma_j) \text{ given below}$$

On substituting (3.19) in the normal force equation, (3.16), and expressing R (the radius of curvature) in terms of derivatives, one gets a second order non-linear equation for the plume surface. Using the variables $\bar{r}$, θ the equation can be written

$$\frac{1}{\bar{r}} \cdot \frac{d^2\bar{r}}{d\theta^2} = \left\{ 1 + \frac{2}{\bar{r}^2} \left(\frac{d\bar{r}}{d\theta} \right)^2 \right\} - \frac{4\bar{r}^2 \sin\theta \cdot (a) \cdot (b)}{(c)}$$

where

$$a = \sin\theta - \frac{\cos\theta}{\bar{r}} \cdot \frac{d\bar{r}}{d\theta}$$

$$b = \frac{\sin^2\theta}{\bar{r}^2} \left(\frac{d\bar{r}}{d\theta} \right)^2 + \frac{2\sin\theta \cos\theta}{\bar{r}} \cdot \frac{d\bar{r}}{d\theta} + \cos^2\theta$$

$$- \frac{\nu(\gamma_j, \theta_M)g^4(\theta)}{2\bar{r}^2}$$

24   MC 62-80-R1

$$c = 2\bar{r}^{-2}\sin^2\theta + \mu(\gamma_j)g^5(\theta)\cdot\frac{(5\cos\theta + \cos\theta_M)}{6}$$

$$\nu(\gamma_j, \theta_m) = \frac{5\mu(\gamma_j)}{2(1-\cos\theta_M)}; \qquad \mu(\gamma_j) = \frac{\dot{m}_j c_j}{\pi y^{*2} p_c}$$

$$g(\theta) = \frac{\cos\theta - \cos\theta_M}{1 - \cos\theta_M}; \qquad = \frac{2\gamma_j}{\sqrt{\gamma_j^2-1}}\left(\frac{2}{\gamma_j+1}\right)^{\frac{1}{\gamma_j-1}}$$

or in functional notation

$$\frac{1}{\bar{r}}\cdot\frac{d^2\bar{r}}{d\theta^2} = F\left\{\bar{r}, \theta, \frac{d\bar{r}}{d\theta}; \gamma_j, \theta_M\right\} \qquad (3.20)$$

This relation contains, in addition to the coordinate variables $(\bar{r},\theta)$, only two explicit parameters, (γ_j, θ_M), and these are fixed by the gas constants of the rocket motor exhaust, and by motor geometry. The effects of all other parameters, i.e., combustion pressure, motor size, forward speed and altitude, are contained implicitly in $\bar{r}$. From the definition

$\bar{r} = (q^o/p_c)^{1/2}(r/y^*)$ it is seen that the operative parameter is $(q^o/p_c)^{1/2}/y^*$,

and that it is simply a scaling factor. For a given motor type, then, a single computation will give the plume shape for all (high) altitudes, all motor sizes, various chamber pressures, and all (supersonic) flight speeds.

It should be emphasized that (3.20) is based on hypersonic flow approximations, and therefore will not apply to the rear portions of the plume where the slopes are of the order of $1/M$ or less. It is also true that in the downstream region of the plume the concept of a layer containing both exterior and interior shocks does not apply; the exterior shock will become an acoustic wave propagating outward at the mach angle, while the inner shock will curve in and remain near the axis (see Fig 3.1). The large region of flow which is thus opened up between them can be analyzed using appropriate techniques, which are those of the linear and second order theories of supersonic flows.

Solutions of (3.20) are presented in the next section. In addition to the positioning of contact surfaces which such solutions represent, it is also possible to derive simplified properties of the double shock layer from the inviscid model. By treating the layer as if it were a mixture of the two gases, instead of being separated by a contact surface, it is possible to estimate the overall thickness of the layer and its average properties. To this end an expression can be written down for $\dot{m}_{ML}$ the mass flow in the merged layer, which is the sum of contributions from the free stream air and the jet; it is given by (see Fig 3.8):

$$\dot{m}_{ML} = \dot{m}_{air \cdot ML} + \dot{m}_{jet \cdot ML}$$

$$= \rho^o U^o \pi r^2 \sin^2\theta + \dot{m}_j \cdot g^5(\theta)$$

or

$$\frac{\dot{m}_{ML}}{\dot{m}_j} = \left\{ \frac{2\overline{r}^2 \sin^2\theta}{(U^o/c_j)\mu(\gamma_j)} + g^5(\theta) \right\} \qquad (3.21)$$

$\mu(\gamma_j)$ as in Eq. 3.20

Using (3.19) and (3.21), V_{ML} can be expressed as

$$\frac{V_{ML}}{c_j} = \mu(\gamma_j) \cdot \left(\frac{\dot{m}_{ML} V_{ML}}{\pi y^{*2} p_c} \right) \left(\frac{\dot{m}_j}{\dot{m}_{ML}} \right) \qquad (3.22)$$

$$= \mu(\gamma_j) \cdot (3.19)/(3.21)$$

The next property to be computed is the weighted average stagnation enthalpy which, neglecting viscosity and heat conduction, is

$$(h_o)_{ML} = \frac{\dot{m}_{air \cdot ML}}{\dot{m}_{ML}} \cdot h_{o \cdot air} + \frac{\dot{m}_{jet \cdot ML}}{\dot{m}_{ML}} h_{o \cdot jet}$$

or

$$\frac{\dot{m}_{ML}(h_o)_{ML}}{\dot{m}_j c_j^2} = \left\{ \frac{(U^o/c_j) \overline{r}^2 \sin^2\theta}{\mu(\gamma_j)} + \frac{g^5}{2} \right\} \qquad (3.23)$$

Because of the relation between stagnation enthalpy, static enthalpy and velocity ($h_0 = h + 1/2V^2$), one gets for the enthalpy of the combined gases in the merged layer:

$$\frac{\dot{m}_{ML} h_{ML}}{\dot{m}_j c_j^2} = (3.23) - \frac{1}{2\mu(\gamma_j)^2} \cdot \frac{(3.19)^2}{(3.21)} \qquad (3.24)$$

The average pressure can be expressed using the notation of the normal force balance (3.13):

$$p_{ML} = \frac{p^o_{ML} + p_{ML,J}}{2}$$

which gives

$$\frac{p_{ML}}{q^o} = 2 \sin^2 \sigma^o - \left(\frac{\dot{m}_{ML} V_{ML}}{\pi y^{*2} p_c}\right)\left(\frac{1}{4\bar{r}\,\bar{R}\,\sin\theta}\right) \tag{3.25}$$

The thickness of the inviscid double shock layer may now be estimated. Using δ_{ML} to indicate thickness measured normal to the plume surface, a mass flow balance gives

$$\dot{m}_{ML} = (2\pi r \sin\theta)\,\delta_{ML}\rho_{ML}V_{ML}$$

or

$$\delta_{ML} = \frac{\dot{m}_{ML}}{2\pi r \sin\theta \cdot \rho_{ML}V_{ML}}$$

Next, using an averaged equation of state

$$\rho_{ML} = \left(\frac{\gamma}{\gamma-1}\right)_{ML} \cdot \frac{p_{ML}}{h_{ML}}$$

the expression for δ_{ML} may be recast in terms of quantities already obtained:

$$\bar{\delta}_{ML} = \frac{\mu(\gamma_j)\,(\frac{\gamma-1}{\gamma})_{ML}}{2\bar{r}\sin\theta} \cdot \left(\frac{\dot{m}_{ML} h_{ML}}{\dot{m}_j c_j^2}\right)\left(\frac{q^o}{p_{ML}}\right)\left(\frac{c_j}{V_{ML}}\right) \tag{3.26}$$

in which the barred quantities are non-dimensional, given by multiplication of $(q^o/p_c)^{1/2}/y^*$ into dimensional quantities. In functional notation 3.26 takes the form

$$\bar{\delta}_{ML} = F\left\{\bar{r},\ \theta;\gamma_j,\ \theta_M,\ (U^o/c_j)\right\}$$

This is similar to the form 3.20 except for the appearance of a new parameter (U^o/c_j) the ratio of free stream velocity to limiting jet velocity. It is interesting to note that this parameter influences the

thickness of the double shock layer but not, according to 3.20, its position. Velocity ratio (U^o/c_j) is equivalent, in the hypersonic approximation to the root of the ratio of stagnation temperatures; specifically

$$U^o/c_j = \left(\frac{C_{P_{air}} T_o}{C_{P_{gas}} T_c} \right)^{1/2}$$

An extension of the analysis will give the individual shock layers, i.e., the properties of the air layer between the contact surface and the outer shock, and the exhaust gas layer on the inside. Assigning the symbol $(\ )_{air}$ to the air layer and $(\ )_{jet}$ to the inner layer, one can write four equations for the two layer thicknesses and the two velocities in the layers. They are

$$\delta_{ML} = \delta_{jet, ML} + \delta_{air, ML}$$

$$\dot{m}_{jet, ML} = 2\pi r \sin \theta \, (\delta_{jet, ML})(\rho_{jet, ML}) \, (V_{jet, ML})$$

$$\dot{m}_{air, ML} = 2\pi r \sin \theta \, (\delta_{air, ML}) \, (\rho_{air, ML}) \, (V_{air, ML})$$

$$\dot{m}_{ML} V_{ML} = (\dot{m}_{jet, ML}) \, (V_{jet, ML}) + (\dot{m}_{air, ML}) \, (V_{air, ML})$$

The above equations are (1) the total thickness, (2) and (3) the mass flow in the air and gas layers, and (4) the total momentum. There are thus four equations for the four unknowns which are soluble by routine algebra. The left sides are all known from the previous formulas; the densities on the right are obtainable from the pressure and enthalpy by equations of state of the same form as given for averaged quantities in the merged layer.

This completes the development of methods for analysis of plume flow in the region of the head, based on inviscid flow theory. Numerical solutions and computations using these methods are described in the next section.

3.4 Solution of the Inviscid Equations

The equation to be solved is (3.20), giving the loci of plume surfaces; it is a second order equation containing a singularity (the denominator (c) of (3.20) passes through zero). The boundary conditions are two in number and are applied at the exit of the rocket motor. The integration is best carried out by machine using standard procedures; that used here is an application of the Runge-Kutta method expressed in R. I. P. language on a ReComp III computer. Numerical results are best

MC 62-80-R1

presented in graphical form showing loci of contact surfaces, singularities, shock layer thicknesses, etc. Before passing to the final results, there are two points to be mentioned which are necessary to the understanding of the integration and the interpretation of the calculations.

The correct boundary conditions must be in accord with the representation of the jet by the formulas of section 3.2. The sketch of Fig. 3.3 shows the situation. A necessary conditic . at the start of computation is, at $\theta = \theta_m$, that $\bar{r} \sin \theta_m$ should equal $(q_o/p_c)^{1/2}$, i.e. that the curve start at the lip of the nozzle. The second condition on the slope is arbitrary. However, by definition a high alti ude plume is such that the value of $(q_o/p_c)^{1/2}$ is very small; the details of how the contact surface starts should not be influential in the final result. Consequently the curve will be started for $\theta = \theta_m$ and $\bar{r} \to$ indefinitely small, a set of conditions which give a determinate solution. The start can be approximated analytically by $\bar{r} = a(\theta_m - \theta)^n$. By substitution in Eq. (3.20) it can be shown that a and n must have the following values:

$$a = \frac{b^2}{3(2 \sin^3 \theta_m)} (\gamma \sin \theta_m - 2 \mu b)^{1/2}$$

where

$$b = (\sin \theta_m)/(1 - \cos \theta_m)$$

γ, μ, as given in (3.20)

$$n = 3$$

These values can be used to start the machine computation at some (small) value of $\bar{r}$, close to $\theta = \theta_m$.

The second question is that of the singularity in Eq. (3.20) when the denominator (c) is zero. Inspection of (c) shows that when $\theta_m < \pi/2$, the value of (c) cannot be zero for finite $\bar{r} \sin \theta$. However, for $\theta_m > \pi/2$ there is a locus of points for (c) = 0 which the plume-curve must cross. By referring to Eq. (3.19) it is seen that (c) = 0 would make the momentum of the merged layer equal to zero unless, at the same point, the slope $\sigma°$ of the contact surface is vertical. Physical reasoning thus requires that the plume curve (contact surface) pass through the locus of singularities vertically. It can be shown that the form of Eq. (3.20) is such that if the plume curve approaches the line of singularities at an angle other than $\pi/2$, the radius of curvature will rapidly become small, turning the curve toward vertical and keeping the second derivative finite; the situation

MC 62-80-R1

has a " static stability. " In practice it was found, in machine calculation, that if the interval of computation did not fall exactly on the line of singularities, then the computation proceeded across the line vertically without special attention. The details will be illustrated by a specific example.

For specific computations, a single value of γ_{jet} will be used: $\gamma_{jet} = 1.25$, corresponding to the value for exhaust gases from a lox - RP - 1 motor. The values of θ_m will be varied in accordance with the following scheme: if it is assumed that exhaust nozzles have parallel flows at the exit, then θ_m can be taken as the maximum Prandtl - Meyer expansion angle for $\gamma_j = 1.25$ and for a Mach number equal to the jet exit Mach number ($M_{J\ EX}$). Varying ($M_{J\ EX}$) will be equivalent to varying θ_m (the relation between $M_{J\ EX}$ and θ_m is shown in Fig. 3.9). Values of $M_{J\ EX}$ of (2, 3, 4, 5) will be used corresponding to θ_m of (150°, 120.5°, 99°, 83°,   ). To apply these results to divergent nozzles it is only necessary to select the proper θ_m and interpolate; the selection of θ_m for rocket nozzles is described in detail in section 3.2.

The first results are shown in Fig. 3.10, which gives the plume shape (contact surface) near the nose for $M_{J\ EX} = 3$. This shape starts out at an angle greater than $\pi/2$, becomes vertical, then starts back; the locus of singularities is drawn in to illustrate the point discussed previously. The coordinates are non-dimensionalized by $(q_o/p_c)^{1/2}/y*$, and denoted by barred quantities.

The next figure (3.11) shows a larger section of the same plume and compares it with the early calculations which neglected centrifugal pressure in the merged layer (equivalent to solving the first order equation (b) = 0, as defined under Eq. 3.20). It appears that the simplified calculations seriously underestimate the size of the plume (30 % - 40 % in terms of nose radius); it also can be shown that the behavior of the contact surface as θ decreases is basically different with the centrifugal term. It is concluded that the centrifugal effects must be accounted for to obtain realistic results.

Fig. 3.12 shows a family of plume contact surfaces for $\gamma_j = 1.25$. A one parameter family is sufficient to represent all possible rocket plumes, at least in the forward regions. The parameter θ_m is tabulated on Fig. 3.12, as well as the corresponding value of the exit Mach number from a non-divergent nozzle. The contact surfaces of Fig. 3.12 may be used as the bases for investigation of the thickness of the inviscid shock layers, the effects of heat conduction and viscosity, and the continuation of the plume flow downstream of the head wave.
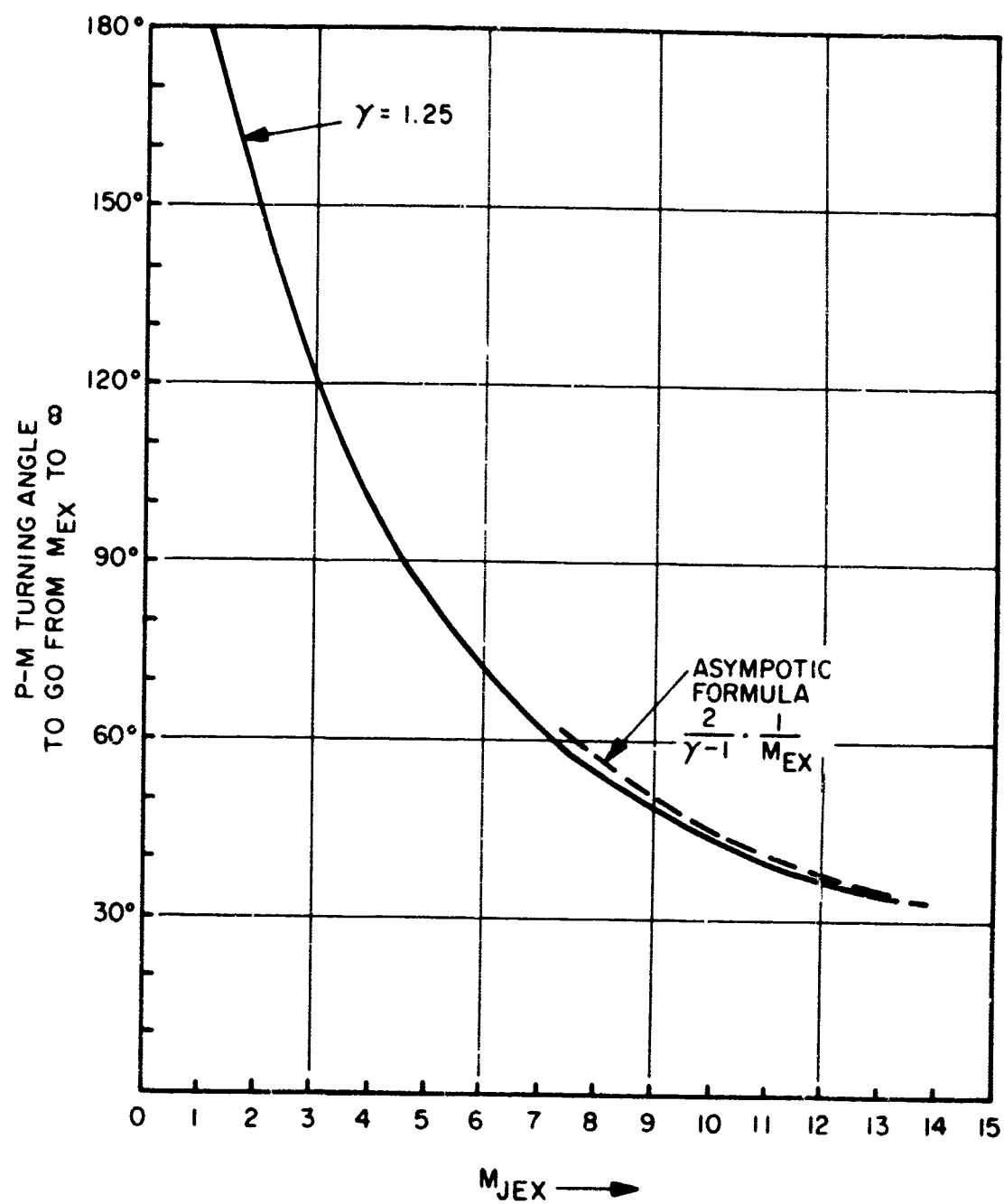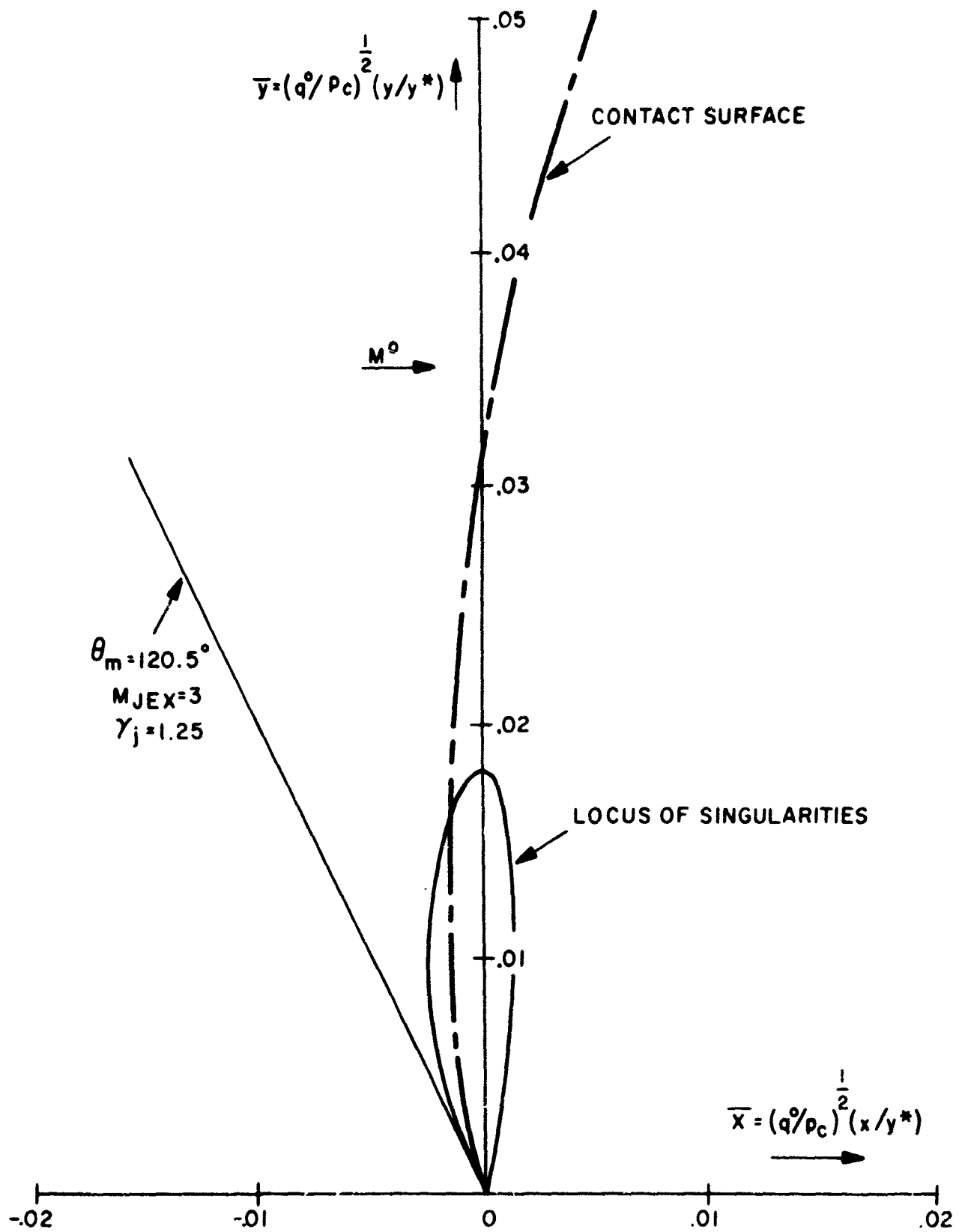
Figure 3.9. Prandtl-Meyer Turning Angles
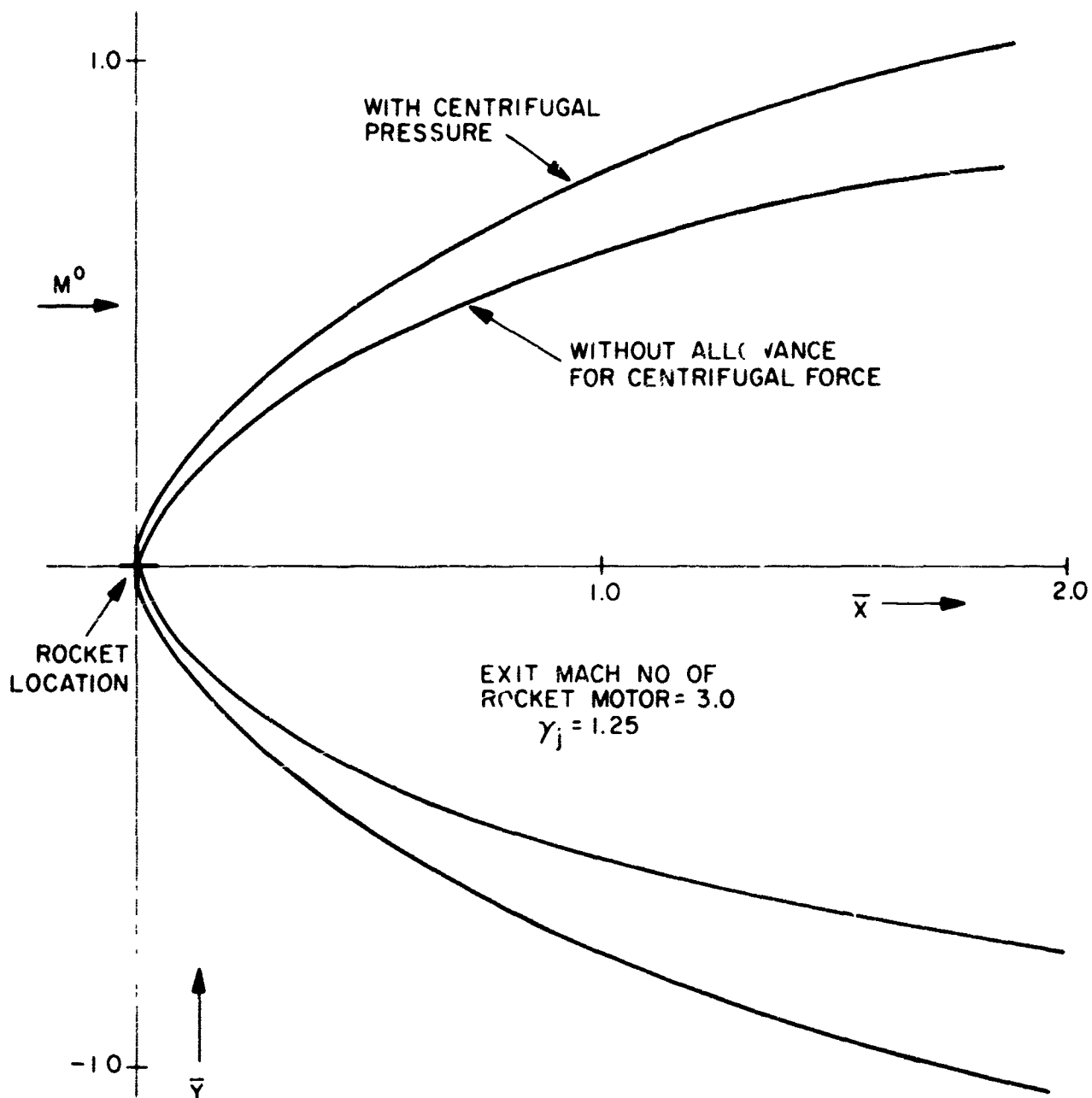
MC 61-80-R1

Figure 3. 10.   Plume Detail Near Origin

MC 63-80-R1

Figure 3.11. Calculated Contact Surfaces at $M_{jex} = 3$
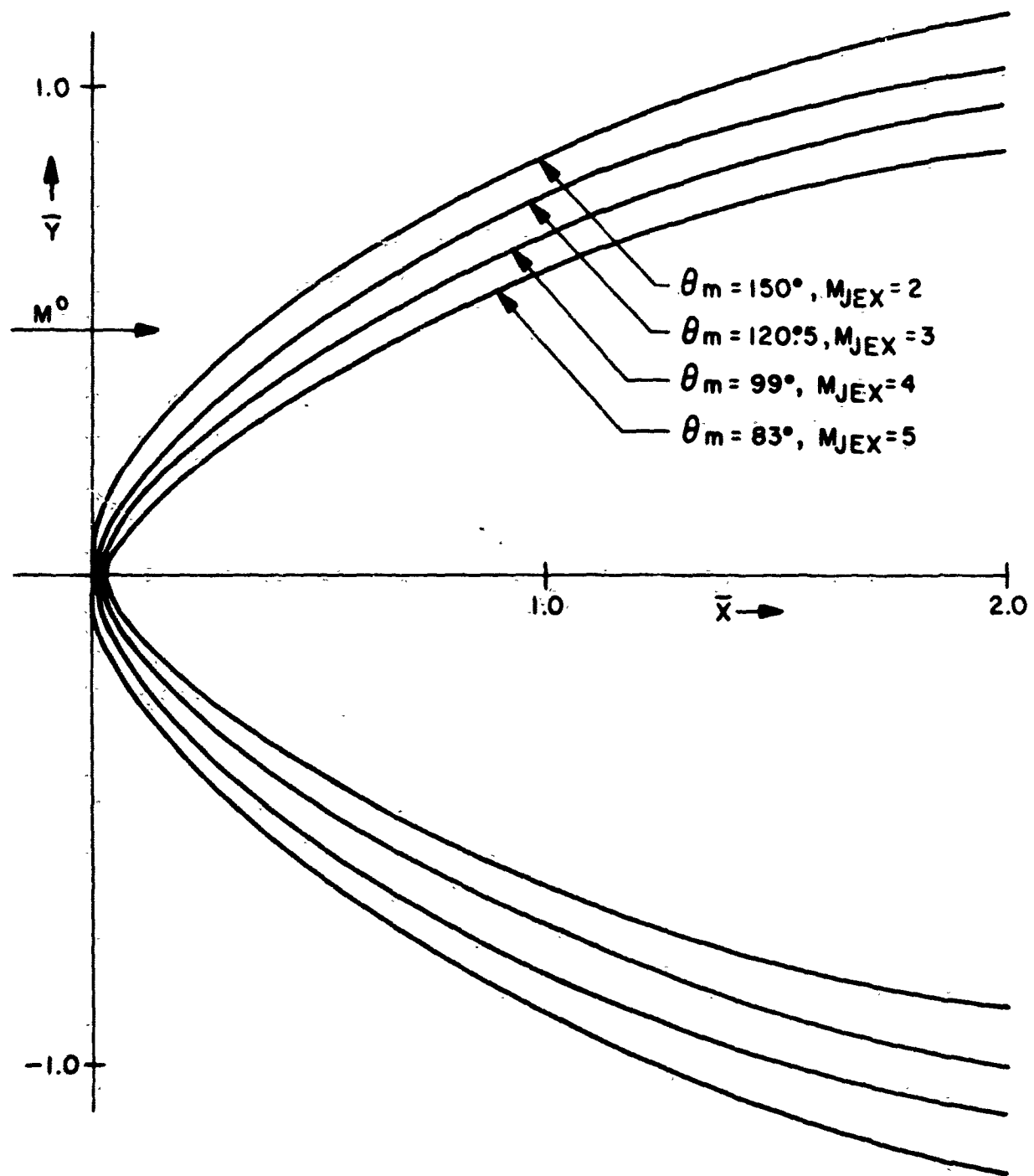
Figure 3.12.   Plume Contact Surfaces γ_j = 1.25

MC 63-80-R1

3.5 Comparison With Flight Data

The technique of Rosenberg et al (1961) provides scaled photographs of the chemiluminescence given off by rocket plumes at night. Assuming that the outer edge of the luminescence defines the outer edge of the gaseous plume, the nose radii as determined by Rosenberg may be compared with those obtained from the calculations. It is assumed that the rocket motor can be represented by the parameter $M_{jex} = 4$ and $\gamma_j = 1.25$, the nominal values for an Atlas sustainer engine.

The effective nose radii of the calculated plumes are determined in a manner similar to that used in obtaining nose radii from photographs. The nose is assumed to be roughly equivalent to a parabola; the parabola constant, which is twice the nose radius, is evaluated by replotting the curves of Fig. 3.12 in terms of y^2 vs x. The slopes are then the parabola constants, as shown in Fig. 3.13. Using the value of R for $M_{jex} = 4$, the nose radius is given theoretically by

$$\frac{R_n}{y^*} = .26 \sqrt{\frac{P_c}{g_o}}, \qquad \gamma^o = 1.4$$
$$\gamma_j = 1.25$$
$$M_{jex} = 4$$

This relationship is plotted on Fig. 3.14 together with the data available from flight. Included among these data are several flights and two different missiles. Also shown is the curve from the blast wave theory of Hill and Habert (1963). It is seen that both theories approximate the data adequately, particularly in view of the uncertainties involved in the data reduction.

3.6 Discussion

It appears that the methods of flow field analysis developed in Section 3 are capable of providing plume shapes in agreement with the known data and with the blast wave theory of Hill and Habert. The flow field technique provides, in addition, formulas for the distribution of thermodynamic properties in the air flow, the jet flow, and the merged layer (as far as inviscid mechanics is applicable). The development here has concentrated on the frontal regions of the plume, since this is the initial disturbance in the creation of the flow pattern. There are standard methods available for continuing the calculation outward and rearward from the frontal regions, as for example those of Witham (1950). The entire flow near the axis (trajectory) is thus subject to analysis by these methods.
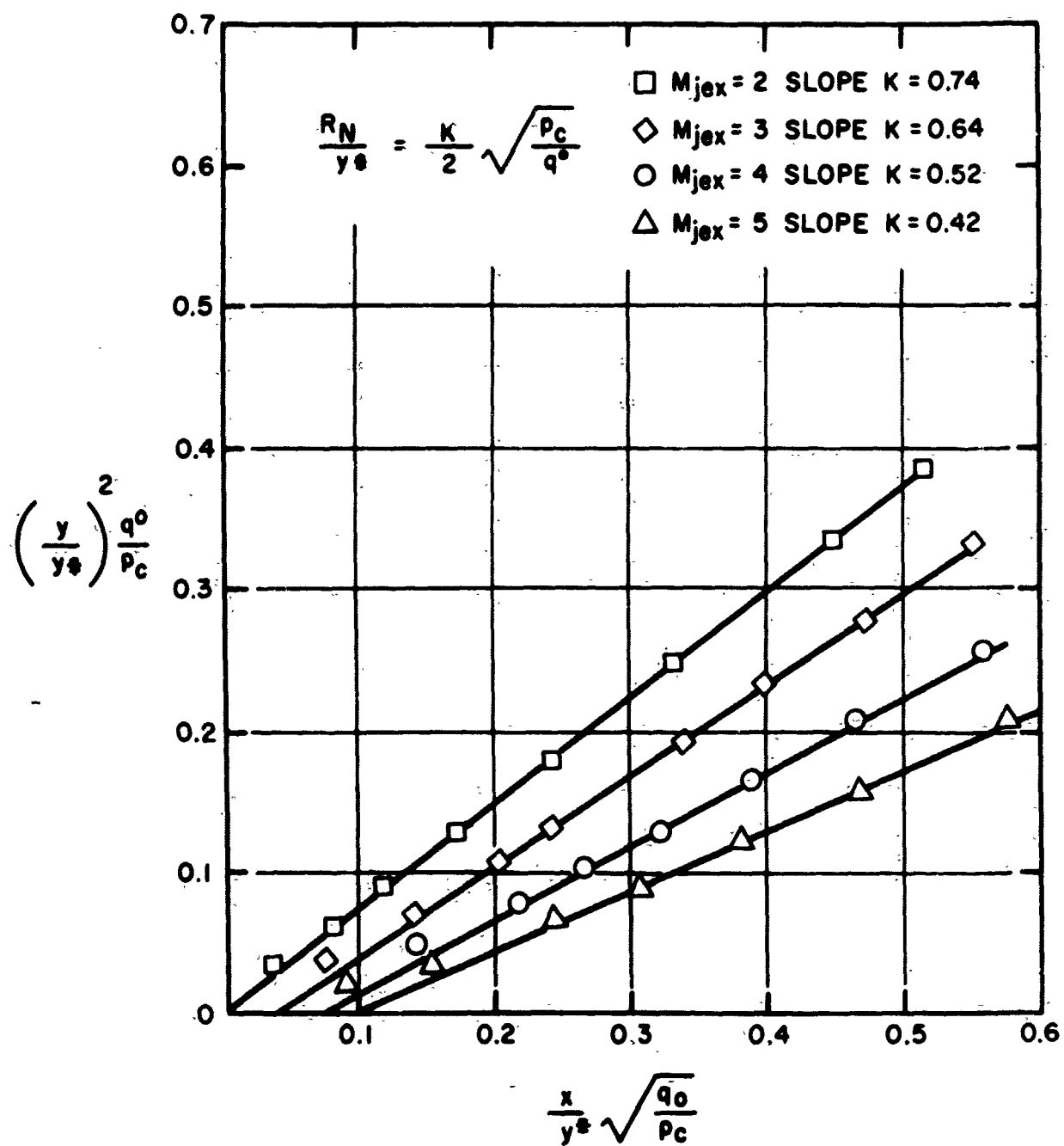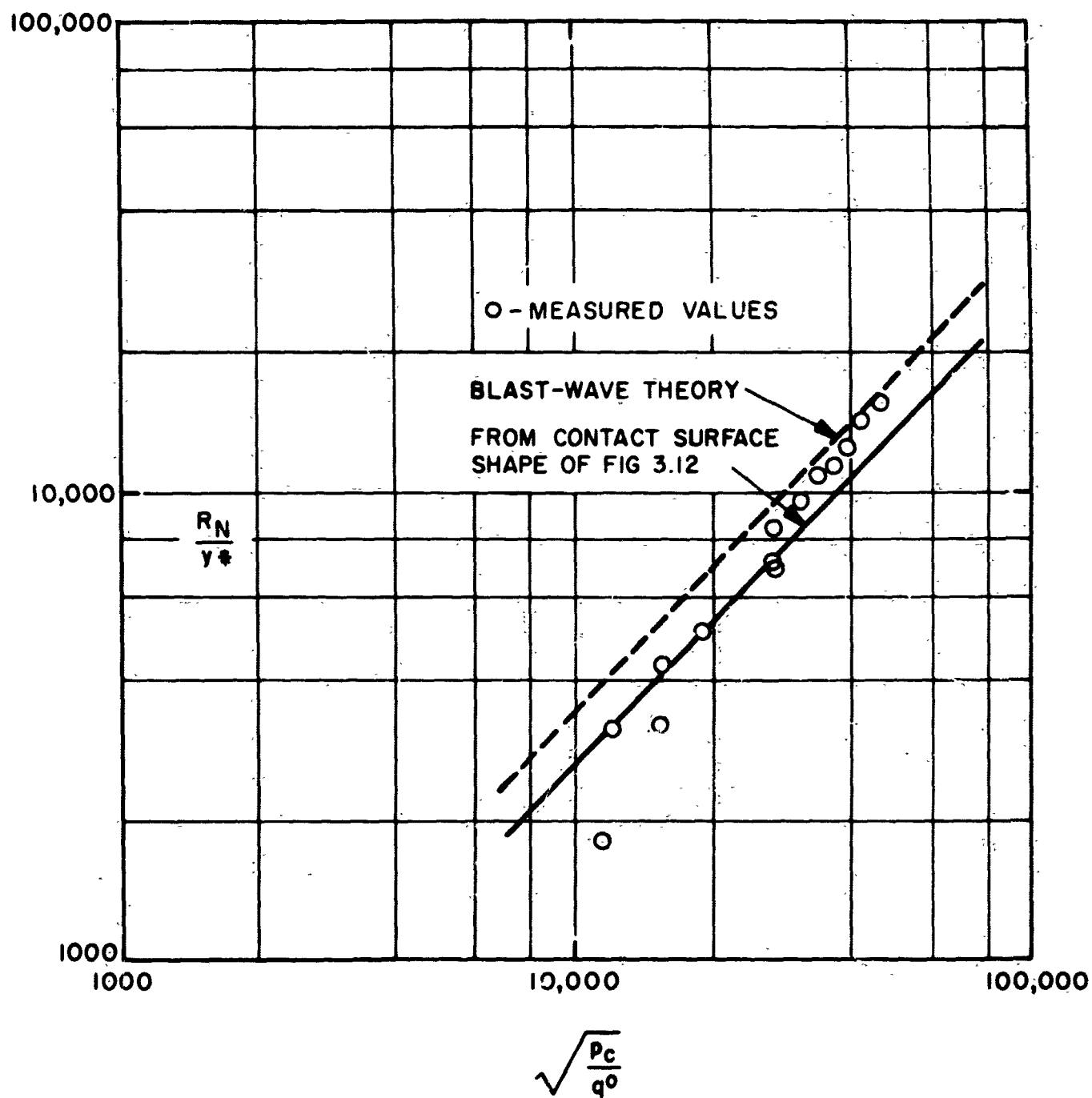
Figure 3.13. Parobola Constants

Figure 3.14. Correlation of Theoretical and Observed Values of
Nose Radii

MC 63-80-P.1

There will be modifications of such calculations which account for the influence and limits of some of the assumptions made here. The estimation of viscous effects must be based on studies of the Navier-Stokes equations as applied to this problem; Section 4 is a detailed investigation into dissipative effects. Another modifying condition is the stratification of the thermodynamic, chemical and electric properties of the atmosphere and their effects on plume flows. In addition the influence of the earth's magnetic field on the electrified particles in the flow becomes relatively larger with increasing height. Finally, proper application of the theory requires some estimation of the limit of validity of continuum mechanics which underlie the present approach. This matter is taken up in Section 5.

MC 63-80-R1

4. MIXING LAYER STRUCTURE AT THE NOSE OF THE PLUME

4.1 General

One important source of observables associated with the high-altitude rocket plume is the mixing of the exhaust gases with the ambient. This mixing occurs in a layer whose mean surface coincides approximately with the contact surface of the inviscid analysis. In this layer the effects of diffusion, viscosity and heat transfer determine the character and properties of the flow. The thickness of the mixing layer is fixed largely by the Reynolds number and a typical plume dimension such as the radius of curvature at the nose. Above 100 Km the Reynolds number is usually less than 100 and the mixing layer fills the entire region between the inner and outer shocks of Fig. 3.1, at least for an appreciable distance back from the nose.

Calcula ions of mixing layers in this flight regime near the limit of continu n flow have not previously been published; the follow-ing analysis represents the first computation of its kind. It is related to several o' "merged-layer" analyses of the flow about solid spheres (Levinsky a... oshihara, 1961; Kao, 1963), but there are several essential differences due to the change in the inner boundary conditions. In the first analysis it is necessary to restrict the study to the region of the nose because of mathematical complexities.

Sections 4.2 and 4.3 present the equations and approximations which are employed to describe the flow in the merged layer. and explain a method which has been developed for solution by numerical integration which exploits a set of asymptotic (analytical) solutions. This method has been selected on the basis of experience with several methods, and is felt to provide the simplest and most easily applied program for obtaining solutions. In the process of developing numerical methods, several sample solutions have been obtained which demonstrate the adequacy of the equations to describe the two thick shocks merged with the mixing zone. In Section 4.4 sample results are presented which were obtained using an earlier method.

4.2 FORMULATION OF THE PROBLEM

The spherical system of reference chosen is depicted in Fig. 4.1. The velocity components are shown in the positive directions. The flow is axisymmetric. The following simplifying assumptions concerning the fluids have been adopted:

(a) The two fluids are two perfect chemically non-reacting gases, with constant specific heats

(b) They diffuse mutually following Fick's law, thus;

$$\rho \vec{v} \cdot \nabla c \; - \; \mathcal{D} \nabla \rho \cdot \nabla c \; - \; \mathcal{D} \rho \nabla^2 c \; = \; 0$$

(c) The Lewis number is unity, and thus the expression for the heat transfer vector is not changed by the mutual diffusion of the two gases.

(d) The Prandtl number is $\frac{3}{4}$

(e) The viscosity coefficient is proportional to the square root of the temperature

4.2.1 Governing Equations

The variables describing the flow field are non-dimensionalized by reference to the upstream conditions according to the following manner:

$$\rho \; = \; \frac{\bar{\rho}}{\rho_\infty} \qquad v \; = \; \frac{\bar{v}}{V_\infty} \qquad u \; = \; \frac{\bar{u}}{V_\infty} \qquad h \; = \; \frac{\bar{h}}{\frac{1}{2}V_\infty^2} \qquad H \; = \; \frac{\bar{H}}{\frac{1}{2}V_\infty^2}$$

$$r \; = \; \frac{\bar{r}}{R} \qquad P_0 \; = \; \frac{\bar{P_0}}{\rho_\infty V_\infty^2} \qquad P_2 \; = \; \frac{\bar{P_2}}{\rho_\infty V_\infty^2} \qquad (4.1)$$

where the symbols with the subscript ∞ denote upstream quantities, and the overlined symbols denote physical variables.

The set of governing equations are:

(a) mass conservation equation

(b, c) radial and tangential Navier Stokes equations

(d) diffusion equation

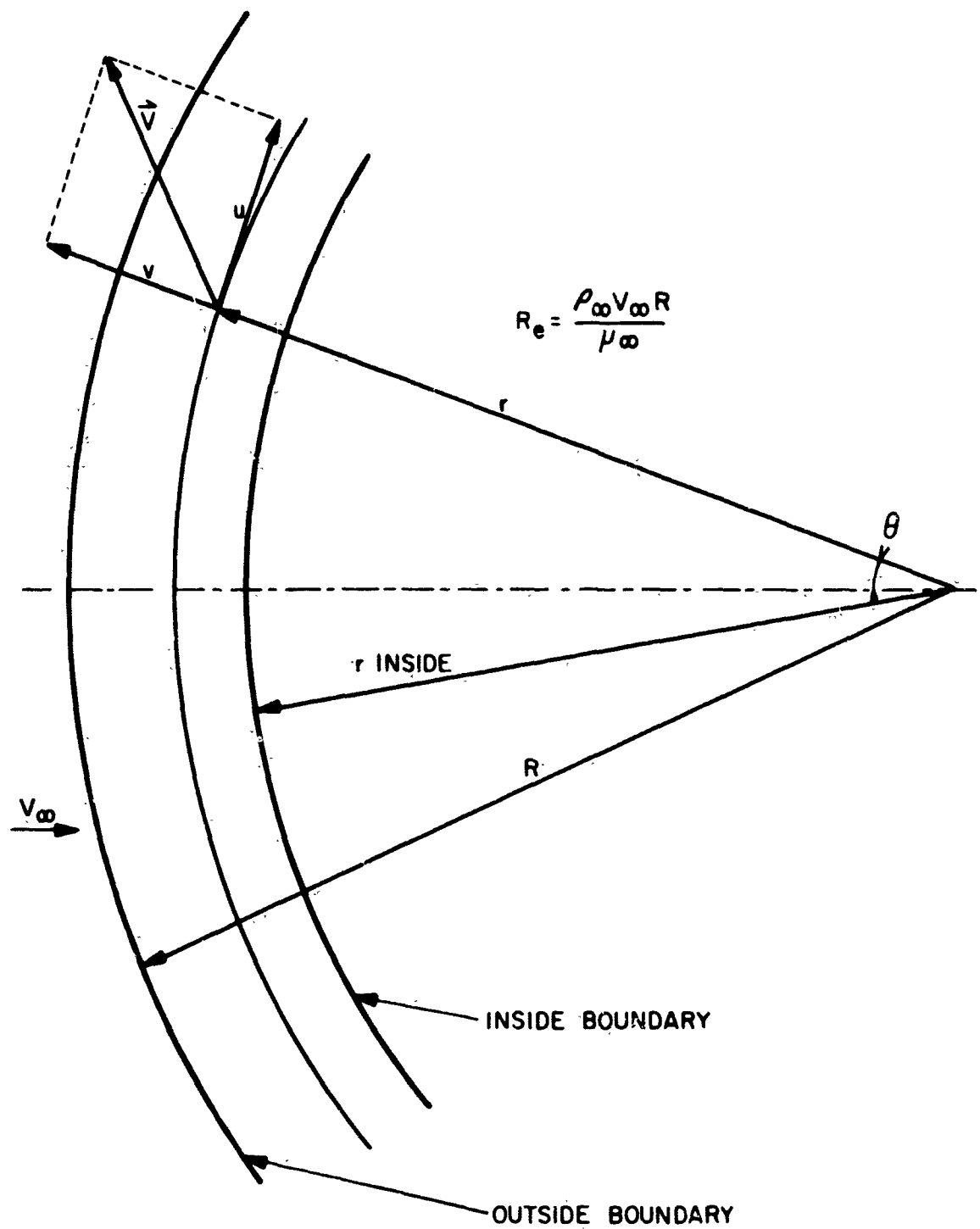MC 63-80-R1

$$R_e = \frac{\rho_\infty V_\infty R}{\mu_\infty}$$

Figure 4.1. Reference System

41

(e) energy equation

(f) equation of state

(g) viscosity law

Explicitly in spherical coordinates they are:

a
$$\left[\frac{1}{r} \frac{\partial}{\partial r} (\rho v r^2) + \frac{1}{\sin\theta} \frac{\partial}{\partial \theta} (\rho u \sin\theta) = 0 \right.$$

b
$$\rho v \frac{\partial v}{\partial r} + \frac{\rho u}{r} \frac{\partial v}{\partial \theta} - \rho \frac{u^2}{r} = -\frac{\partial p}{\partial r} +$$

$$\frac{1}{Re} \left\{ \frac{\partial}{\partial r} \left[\mu \frac{\partial v}{\partial r} - \frac{1}{3} \frac{\mu}{r} (r \frac{\partial v}{\partial r} + 2v + \frac{\partial u}{\partial \theta} + u \cot\theta) \right] \right.$$

$$+ \frac{1}{r} \frac{\partial}{\partial \theta} \left[\mu (r \frac{\partial}{\partial r} (\frac{u}{r}) + \frac{1}{r} \frac{\partial v}{\partial \theta}) \right] + \frac{2\mu}{r} (2 \frac{\partial v}{\partial r} - \frac{v}{r} - \frac{1}{r} \frac{\partial u}{\partial \theta})$$

$$\left. + \frac{\mu}{r} \left[\cot\theta (r \frac{\partial}{\partial r} (\frac{u}{r}) + \frac{1}{r} \frac{\partial v}{\partial \theta}) - \frac{2}{r} (v + u \cot\theta) \right] \right\}$$

c
$$\rho v \frac{\partial u}{\partial r} + \frac{\rho u}{r} \frac{\partial u}{\partial \theta} + \frac{\rho uv}{r} = -\frac{1}{r} \frac{\partial p}{\partial \theta} \qquad (4.2)$$

$$+ \frac{2}{r} \frac{\partial}{\partial \theta} \left[\frac{\mu}{r} (v + \frac{\partial u}{\partial \theta}) - \frac{1}{3} \frac{\mu}{r} (r \frac{\partial v}{\partial r} + 2v + \frac{\partial u}{\partial \theta} + u \cot\theta) \right]$$

$$+ \frac{\partial}{\partial r} \left\{ \mu \left[r \frac{\partial}{\partial r} (\frac{u}{r}) + \frac{1}{r} \frac{\partial v}{\partial \theta} \right] \right\} + 3 \frac{\mu}{r} \left[r \frac{\partial}{\partial r} (\frac{u}{r}) + \frac{1}{r} \frac{\partial v}{\partial \theta} \right]$$

$$+ 2 \frac{\mu}{r^2} \cot\theta \left[\frac{\partial u}{\partial \theta} - u \cot\theta \right]$$

d
$$\rho v \frac{\partial c}{\partial r} + \frac{\rho u}{r} \frac{\partial c}{\partial \theta} = \frac{4}{3} \frac{1}{Re} \left\{ \frac{\partial}{\partial r} (\mu \frac{\partial c}{\partial r}) + \frac{1}{r^2} \frac{\partial}{\partial \theta} (\mu \frac{\partial c}{\partial \theta}) \right.$$

$$\left. + \mu \left[\frac{2}{r} \frac{\partial c}{\partial r} + \frac{\cot\theta (1 - 2 \sin^2\theta)}{r^2} \frac{\partial c}{\partial \theta} \right] \right]$$

e
$$2(\rho v \frac{\partial H}{\partial r} + \rho \frac{u}{r} \frac{\partial H}{\partial \theta}) = \left\{ 2 \left\{ v \frac{\partial}{\partial r} \left[\mu \frac{\partial v}{\partial r} \right] + \frac{u}{r^2} \frac{\partial}{\partial \theta} \left[\mu(v + \frac{\partial u}{\partial \theta}) \right] \right. \right.$$

$$\left. + \mu \left[(\frac{\partial v}{\partial r})^2 + \frac{1}{r^2} (v + \frac{\partial u}{\partial \theta})^2 \right] \right\}$$

$$- \frac{2}{3} \left[(v \frac{\partial}{\partial r} + \frac{u}{r} \frac{\partial}{\partial \theta}) (\mu F) + \mu F^2 \right] + (\frac{v}{r} \frac{\partial}{\partial \theta} + u \frac{\partial}{\partial r})$$

$$\left[\mu (r \frac{\partial}{\partial r} (\frac{u}{r}) + \frac{1}{r} \frac{\partial v}{\partial \theta}) \right]$$

42

$$+ \frac{\mu v}{r} \left[4 \frac{\partial v}{\partial r} - \frac{2}{r} (v + \frac{\partial u}{\partial \theta}) + \cot \theta \left[r \frac{\partial}{\partial r} (\frac{u}{r}) + \frac{1}{r} \frac{\partial v}{\partial \theta} \right] \right.$$

$$\left. - \frac{2}{r} (v + u \cot \theta) \right]$$

$$+ \frac{\mu u}{r} \left[3 (r \frac{\partial}{\partial r} (\frac{u}{r}) + \frac{1}{r} \frac{\partial v}{\partial \theta}) + \frac{2}{r} \cot \theta (\frac{\partial u}{\partial \theta} - u \cot \theta) \right]$$

e

$$+ \mu \left[\frac{2}{r^2} (v + u \cot \theta)^2 + r^2 \left[\frac{\partial}{\partial r} (\frac{u}{r}) \right]^2 + \frac{1}{r^2} (\frac{\partial v}{\partial \theta})^2 \right.$$

$$\left. + \frac{\partial}{\partial r} (\frac{u}{r}) \frac{\partial v}{\partial \theta} + \frac{1}{r} \frac{\partial u}{\partial r} \frac{\partial v}{\partial \theta} \right]$$

$$+ \frac{1}{r} \frac{4}{3} \left[\frac{\partial}{\partial r} \left[\mu r \frac{\partial h}{\partial r} \right] + \frac{\partial}{\partial \theta} (\frac{\mu}{r} \frac{\partial h}{\partial \theta}) + \mu \frac{\partial h}{\partial r} + \mu \frac{\cot \theta}{r} \frac{\partial h}{\partial \theta} \right] \right\} \frac{1}{Re}$$

where

$$\begin{cases} F = \frac{\partial v}{\partial r} + \frac{1}{r} \frac{\partial u}{\partial \theta} + \frac{2v}{r} + \frac{u}{r} \cot \theta \\[2ex] H = h + v^2 + u^2 \end{cases}$$

(4.2 Cont)

f $\left[P = \Gamma \rho h \right.$

where

$$\Gamma = \frac{1}{2} \frac{R_{air} + (R_{gas} - R_{air}) c}{C_{P_{air}} + (C_{P_{gas}} - C_{P_{air}})c}$$

g $\left[\dfrac{\mu}{\mu_\infty} = (\dfrac{h}{h_\infty})^{\frac{1}{2}} \right.$

4.2.2 Separation of Independent Variables

The present method of separating the independent variables has been used by several investigators (Hays 1959, Levinsky 1961, Kao 1963):

$$v = v_o \cos \theta$$

$$u = u_1 \sin \theta$$

$$\rho = \rho_o$$

$$\mu = \mu_o \cos \theta$$

43   MC 63-80-R1

$$h \quad = \quad h_o \cos^2 \theta$$

$$H \quad = \quad H_o \cos^2 \theta$$

$$p \quad = \quad p_o \cos^2 \theta \; + \; p_2 \sin^2 \theta \qquad\qquad (4.3)$$

The quantities with a subscript are functions of r only.

4.2.3 Derivation of the Reduced Equations

In the system of governing equations the terms of order smaller than Δ/R or μ/Re are neglected (Δ is the thickness of the layer).

The expressions assumed for the separation of independent variables are substituted into the full system and yield the following set of reduced equations, the only independent variable being r.

$$(\rho v)' \; + \; \frac{2\rho}{r} \, (u + v) \; = \; 0 \qquad\qquad \text{Continuity}$$

$$\rho v v' \; + \; p_o' \; = \; \frac{1}{Re} \; \left(\frac{4}{3} \, \mu v' \right)' \qquad\qquad \text{Rad. Mom(1)}$$

$$p_2' \; = \; \frac{\rho u}{r} \, (u + v) \qquad\qquad \text{Rad. Mom(2)}$$

$$\rho v u' \; + \; \frac{\rho u}{r} \, (u + v) \; + \; \frac{2}{r} \, (p \quad p_o) \; = \; \frac{1}{Re} \, (\mu u')' \qquad \text{Tan. Mom}$$

$$\rho v c' \; = \; \frac{1}{Re} \; \frac{4}{3} \; (\mu c')' \qquad\qquad \text{Diffusion}$$

$$\rho v H' \; = \; \frac{1}{Re} \; \frac{4}{3} \; (\mu H')' \qquad\qquad \text{Energy}$$

$$p_o \; = \; \Gamma \rho h \qquad\qquad \text{1st State}$$

$$\mu \; = \; \left[\frac{h}{c \, \dfrac{2 C_{p_{gas}} T_\infty}{V_\infty^2} \; + \; (1-c) \, \dfrac{2}{\gamma - 1} \; \dfrac{1}{M_\infty^2}} \right]^{\frac{1}{2}} \qquad \text{Viscosity}$$

$$(4.4)$$

$$H = h + v^2 \qquad\qquad \text{Tot. Enthalpy}$$

As a matter of convenience the variables appearing in (4.3) are denoted without indexes when the meaning of the symbol can be determined without ambiguity. This convention is carried on henceforth.

44

MC 63-80-R1

4.2.4 Boundary Conditions

The matching of the outside flow specifies the following variables

$$\rho = 1 \qquad v = -1 \qquad u = 1 \qquad c = 0 \qquad h = \frac{2}{\gamma_A - 1} \, \frac{1}{M_\infty^2}$$

$$P_2 = P_0$$

which in turn prescribe

$$H = 1 + \frac{2}{\gamma_A - 1} \, \frac{1}{M_\infty^2} \qquad\qquad P_0 = \frac{1}{\gamma_A \, M_\infty^2} \qquad\qquad (4.5)$$

The boundary conditions in the inner edge are given by the inner source flow. The inviscid system of equations is:

$$(\rho v)' \quad + \quad \frac{2\rho}{r} (u + v) = 0$$

$$\rho v v' \quad + \quad P_0' = 0$$

$$P_2' \quad = \quad \frac{\rho u (u + v)}{r} \qquad\qquad (4.6)$$

$$P_0 \quad = \quad \Gamma \rho (H - v^2)$$

$$\rho v u' \quad + \quad \frac{\rho u (u + v)}{r} + \frac{2}{r} (P_2 - P_0) = 0$$

$$H' \quad = \quad 0$$

$$c' \quad = \quad 0$$

This yields rigorously:

$$H \quad = \quad H_G$$

$$c \quad = \quad \text{Constant}$$

$$\frac{\rho}{(H - v^2)^{\frac{1}{\gamma_G - 1}}} \quad = \quad \text{Constant} \qquad\qquad (4.7)$$

The expression of the third constant deserves some attention. The entropy of a perfect gas is given by the differential expression:

$$dS = R_{per}\left[\frac{1}{\gamma - 1}\frac{d\bar{h}}{\bar{h}} + \frac{d\bar{v}}{\bar{v}}\right]$$

where S and $\bar{v}$ designate entropy and specific volume respectively. dS is independent of the mode of non dimensionalization, and hence:

$$dS = R_{per}\left[\frac{1}{\gamma - 1}\frac{dh}{h} + \frac{dv}{v}\right]$$

or

$$\frac{S - S_o}{R_{per}} = \ln\frac{h}{\rho}^{\frac{1}{\gamma - 1}}$$

S_o being an arbitrary constant which will be taken as zero. The application of this definition at the inside boundary yields a physical meaning to the third constant;

$$\frac{\rho}{(H - v^2)^{\frac{1}{\gamma_G - 1}}} = e^{-\frac{S_G}{R_G}}$$

where S_G is the enthalpy of the gas. The two constants H_G and S_G are provided by the characteristic features of the source. The specific application of these conditions to the numerical solutions will be made in section 4.3.4. It should be noted that the last condition is equivalent to saying that the flow becomes isentropic along the axis of flow.

4.3 SOLUTION OF THE EQUATIONS

4.3.1 Reduction to First Order Equations

By introducing the new variables

$$\phi = \mu H'; \quad W = \mu v'; \quad \chi = \mu C'; \quad \omega = \mu u'$$

the system of reduced equations of the last section may be recast as the following system of ten first order equations:

$$v\rho' = -\rho\left\{\frac{2(u+v)}{r} + \frac{W}{\mu}\right\} \tag{4.8}$$

$$v' = W/\mu$$

$$u' = \omega/\mu$$

$$C' = \chi/\mu$$

$$P_2' = \rho u(u+v)/r$$

$$\chi' = (3/4)\mathrm{Re}\,(\rho v\chi)/\mu$$

$$W' = (3/4)\mathrm{Re}\,(p_0' + \rho vv')$$

$$\omega' = \mathrm{Re}\left\{\rho\left[(v\omega)/\mu + u(u+v)/r\right] + 2(p_2 - p_0)/r\right\}$$

and

$$H_0' = \phi/\mu$$

$$\phi' = (3/4)\mathrm{Re}(\rho v\phi)/\mu$$

The ten unknown variables appear as first derivatives on the left side of the equations. The quantities μ and p_0 on the right side are not to be considered as additional unknowns, but as functions of the ten primary unknowns; they are given algebraically in terms of the latter by

$$P_0 = \Gamma\rho h_0 \tag{4.9}$$

$$\mu = \left[\frac{h_0}{\dfrac{2C_{P_{gas}}T_\infty}{V_\infty^2}\,C + (1-C)\dfrac{2}{(\gamma_{air}-1)M_\infty^2}}\right]^{\frac{1}{2}}$$

where

$$h_0 = H_0 - v^2$$

$$\Gamma = \frac{1}{2}\,\frac{C\,R_{gas} + (1-C)\,R_{air}}{C\,C_{P_{gas}} + (1-C)\,C_{P_{air}}}$$

In the general case this system of equations requires specification of ten constants of integration. If these can be determined at one point through a knowledge of the values of the dependent variables at that point, then a solution of the equations is, in principle, determined. The problem treated here however has some conditions given at the outer boundary and the rest at the inner boundary. The handling of this two-point boundary value problem requires special attention, and is discussed in the next section.

The ten equations may be reduced to eight by extracting two integrals from the system. The equations for χ' and ϕ' may be combined to give

so

$$\phi'/\phi = \chi'/\chi$$

$$\phi = k_1 \chi$$

Using the equations for C' and H', this last becomes

or

$$H'_o = k_1 C'$$

$$H_o = k_1 C + k_2 \tag{4.10}$$

This relation may be considered as another algebraic equivalence of the type (4.9); with it H_o may be eliminated as an unknown. The equation for H'_o may be dropped, as well as the equation for ϕ' since ϕ appears only in the equations for H'_o and ϕ'. This leaves eight equations (the first eight of the set (4.8), and eight unknowns (appearing as first derivatives in the left column), and eight arbitrary constants of integration. The two constants k_1 and k_2 of (4.10) are arbitrary and complete the total of ten. It should be noted that the linear dependence of total energy on concentration is a special result of picking the Prandtl number to be $3/4$.

The values of k_1 and k_2 are determined from two of the boundary conditions given in the previous section. One condition is at the outer boundary, the other at the inner. Specifically

$$k_1 = H_G - k_2$$

$$k_2 = 1 + \frac{2}{(\gamma_A - 1)} \cdot \frac{1}{M_\infty^2} \tag{4.11}$$

where

γ_A = ratio of specific heats in the ambient

H_G = total enthalpy of inner flow; this is the constant of the first equation in (4.7).

The integration of the eight equations can now proceed providing a method is adopted which overcomes the problem of two-point boundary values. A second problem will be encountered at the stagnation point (where v becomes zero) owing to the nature of the first equation of the set (4.8). It can be seen that the value of ρ' will become either infinite or indeterminate.

The two point boundary problem will be dealt with by using the method of asymptotic solutions at the outer boundary, and is taken up in the next section. The solution near stagnation will be obtained by series expansion, and is described in section 4.3.3.

4.3.2 Asymptotic Solutions at the Outer Boundary

The method of asymptotic solutions is to linearize the equations at the outer boundary, where the unknowns may be expressed as small perturbations from the limiting boundary values. The resulting equations can then be solved by standard methods. The solutions will include ten arbitrary constants corresponding to the ten boundary conditions of the problem. As will be shown, seven can be imposed in advance on the basis of boundary values, while another can be fixed in advance by relating it to the Reynolds number selected for the computation. The remaining two can only be picked by relating them to the inner flow through numerical integration across the merged layer. How this may be done is detailed in this and the next section.

The asymptotic forms may be written as follows, using Δ as a modifier to indicate small quantities:

$$\rho = 1 + \Delta\rho \qquad\qquad p_2 = (1/\gamma_A M_\infty^2) + \Delta p_2$$
$$v = -1 + \Delta v \qquad\qquad X = \Delta X$$
$$u = 1 + \Delta u \qquad\qquad W = \Delta W$$
$$C = \Delta C \qquad\qquad \omega = \Delta\omega \qquad\qquad (4.12)$$

These forms are substituted in the set of eight equations (4.8); eight linear equations are obtained by rejecting terms of second and higher orders. The result is

$$\Delta\rho = \left\{ \frac{2(\Delta u + \Delta v)}{r} + \Delta W \right\} \qquad\qquad (4.13)$$

$$\Delta v' = \Delta W; \quad \Delta C' = \Delta X; \quad \Delta X' = -\left(\frac{3}{4}\right) Re \cdot \Delta X$$

$$\Delta u' = \Delta\omega; \quad \Delta p_2' = \frac{(\Delta u + \Delta v)}{r}; \quad \Delta W' = \left(\frac{3}{4}\right) Re(\Delta p_o' - \Delta W)$$

$$\Delta\omega = Re\left\{ -\Delta\omega + \frac{(\Delta u + \Delta v)}{r} + \frac{2}{r}(\Delta p_2 - \Delta p_o) \right\}$$

49

The linearized algebraic relations corresponding to (4.9) are

$$\Delta p_o = A \cdot \Delta C + \left(\frac{1}{\gamma_A M_\infty^2}\right)\Delta \rho + \left(\frac{\gamma_A - 1}{\gamma_A}\right)\Delta v$$

$$A = \left\{\frac{2}{(\gamma_A - 1)M_\infty^2}\left(\frac{di'}{dC}\right)_{C=0} + k_1\left(\frac{\gamma_A - 1}{2\gamma_A}\right)\right\} \quad (4.14)$$

$$\left(\frac{d\Gamma}{dC}\right)_{C=0} = \frac{1}{2}\frac{C_{p_{gas}}}{C_{p_{air}}}\left\{\left(\frac{\gamma_A - 1}{\gamma_A}\right) - \left(\frac{\gamma_G - 1}{\gamma_G}\right)\right\}$$

k_1 from eq. 4.11

$$p_o = \frac{1}{\gamma_A M_\infty^2} + \Delta p_o$$

$$\mu = 1 + \Delta\mu \ , \quad \Delta\mu \text{ not needed.}$$

Now the equations for $\Delta X'$ and $\Delta C'$ can be solved independently; they yield

$$\Delta X = -(3/4)Re \ k_3 e^{-(3/4)Re \ r}$$

$$\Delta C = \int \Delta X dr = k_3 e^{-(3/4)Re \ r} + k_4 \quad (4.15)$$

$$\text{where } k_4 = 0$$

Another integration is possible by combining equations for ρ', v' and p_2':

$$+\Delta\rho' = 2\Delta p_2' + \Delta v' \quad (4.16)$$

$$\Delta p_2 = \frac{\Delta\rho - \Delta v}{2} + k_5$$

$$\text{where } k_5 = 0$$

These results may be used to reduce the set (4.13) to three equations for three unknowns. It is convenient at the same time to redefine the independent variable to be $\tau = r \, Re$ and the symbol for differentiation to be $d/d\tau = (\ )^\nabla = (\ )'/Re$. The three equations for Δu, Δv and $\Delta\rho$ are

(a) $\quad \Delta\rho^\nabla - \Delta v^\nabla = \dfrac{2(\Delta u + \Delta v)}{\tau}$

(b) $\quad \Delta v^{\nabla\nabla} = \dfrac{3}{4}(\Delta p_o^\nabla - \Delta v^\nabla)$ $\quad (4.17)$

(c) $\quad \Delta u^{\nabla\nabla} + \Delta u^\nabla = \dfrac{1}{\tau}\left\{\Delta u + \Delta\rho - 2\Delta p_o\right\}$

MC 63-80-R1

It should be noted that Re does not appear explicitly in this set. These relations, although linear and comparatively simple, cannot be solved exactly in closed form. Useful solutions are obtained by noting that in the regions of interest we have $\tau > 10$, and that what is needed is the behavior of u, v and ρ as $\tau \to \infty$. This suggests a series expansion of the solution in reciprocal powers of τ, having the following form:

$$\Delta u = \sum_{n=0}^{\infty} (\frac{1}{\tau})^p (\frac{1}{\tau})^n [\Delta u]_n$$

In this expression, the $[\Delta u]_n$ are functions of τ, and will turn out to be solutions of linear equations with constant coefficients. The power p is included to account for the fact that some solutions are not expressible as integral powers of $(1/\tau)$, and require a fractional power; p is taken to lie between 0 and 1. Its specific value is determined when Δu is substituted in (4. 17), together with similar expressions for $\Delta \rho$ and Δv. Because of the large values of τ it will be sufficient to carry the determination of the $[\Delta u]_n$ only so far as is necessary to bring in the arbitrary constants of integration; thus will turn out to be only the zero order terms for $\Delta \rho$ and Δv, and the zero and first order for Δu. Inspection of the set (4. 17) shows that there will be five arbitrary constants of integration. One is determined at once by single integration of (b); calling it k_0, it is seen at once that $k_6 = 0$ is required by the boundary conditions. Of the remaining four, two will not be determined by the outer boundary conditions; the significant solutions of (4. 17) will contain these two arbitrary constants. The equations for the zero order terms result from direct substitution, and are (for any value of p)

$$[\Delta \rho]_o^{\nabla} - [\Delta v]_o^{\nabla} = 0$$

$$[\Delta v]_o^{\nabla} = \frac{3}{4} \left\{ [\Delta \rho_o]_o - [\Delta v]_o \right\}$$

$$[\Delta u]_o^{\nabla \nabla} + [\Delta u]_o^{\nabla} = C$$

($[\Delta \rho_o]_o$ and ΔC from 4-14 and 4-15)

These expressions have constant coefficients and their solutions are easily obtained. They are

$$[\Delta \rho]_o = [\Delta v]_o + k_7$$

$$[\Delta v]_o = k_8 e^{-\frac{3B^2}{4} \tau}, \quad -\frac{A}{1 - B^2} \Delta C \qquad (4.18)$$

$$[\Delta u]_o = k_9 e^{-\tau}, \quad k_{10}$$

where $\qquad B^2 = \dfrac{M_\infty^2 - 1}{\gamma_A M_\infty^2}$

Each of these terms has yet to be multiplied by its respective $(1/\tau)P$. To determine the p's it is necessary to examine the higher order terms; it is found that the solution cannot be continued unless, for the k_9 term, $p = 1$; and for the k_8 term, $p = 2/(M_\infty^2 - 1)$. For the constant terms, k_7 and k_{10} there are no values of p which will permit the solution to be continued in a convergent series, and hence they are zero. This completes the information needed for the asymptotic solutions, which can now be written out explicitly:

$$\Delta u = \frac{1}{\tau}\left\{ k_9 e^{-\tau} + \frac{16}{3}k_3 A\left[2 + \frac{C}{(B^2 - 1)}\right]e^{-(3/4)\tau} + \frac{C\,k_8}{\frac{3}{4}B^2(1 - \frac{3}{4}B^2)\tau^P}e^{-(3/4)B^2\tau}\right\} + \frac{1}{\tau^2}\left\{ \cdots\right.$$

$$\Delta v = \left\{ \frac{k_3 A}{B^2 - 1}e^{-(3/4)\tau} + \frac{k_8}{\tau^P}e^{-(3/4)B^2\tau}\right\} + \frac{1}{\tau}\left\{ \cdots\right.$$

$$\Delta \rho = \left\{ \frac{k_3 A}{B^2 - 1}e^{-(3/4)\tau} + \frac{k_8}{\tau^P}e^{-(3/4)B^2\tau}\right\} + \frac{1}{\tau}\left\{ \cdots\right.$$

$$\Delta C = k_3 e^{-(3/4)\tau} \tag{4.19}$$

A from 4.14; B from 4.18; $C = \dfrac{2 - (2 - \gamma_A) M_\infty^2}{\gamma_A M_\infty^2}$

$$P = \frac{2}{M_\infty^2 - 1}, \quad M > \sqrt{3}$$

There are three constants (k_3, k_8 and k_9) of integration which are still undetermined. The seven already determined are essentially fixed by the six independent conditions at the outer boundary and one (total enthalpy) of the inner flow. Thus k_3, k_8, and k_9 are related to the as yet un-specified character of the inner flow. One condition can be applied as follows: select a Reynolds number based on the distance from the origin to the outer boundary as determined, say, by the value of τ at that point where the density is 1% above free stream value; then setting Re $= \tau$ and $\Delta \rho = .01$ in the asymptotic formula, a condition is obtained on k_3 and k_8. This condition essentially fixes the scale of the flow; with it one of the constants say k_8, can be eliminated. The two remaining conditions are obtainable only by picking trial values of the k_3 and k_9, integrating the equations numerically through the merged layer and thus relating the constants in the asymptotic solution to the properties of the

inner flow. To match a given inner flow it will be necessary to choose two constants at the outer edge which give two specified properties of the inner flow (in addition to the stagnation enthalpy, which is already determined). This process is essentially the inversion of a rank two matrix and presents no real problem once a series of integrations has been carried out. A discussion of the integration through the stagnation point and the inner flow properties follows.

4.3.3 The Solution Near Stagnation

As noted in the previous section, the expression for ρ' in the set 4.8 becomes singular when $v = 0$. In numerical integration by machine the consequence is an instability of computation near stagnation. A method of extrapolating across the unstable band may be developed based on a series expansion about this point. It is first useful to select a point in the computation which is near the point of $v = 0$ but before instability appears, and this requires a criteria. From the first equation of (4.8) it is seen that both v and the bracket on the right should pass through zero linearly with r, and at the same point. Using a scheme of linear extrapolation, the point where $v = 0$ is estimated by

$$0 = v + v'\eta$$

$$0 = v + \frac{W\eta}{\mu}$$

where

so

$$r = r_o + \eta \ , \ r_o = \text{point at which } v = 0$$

$$\eta = -\frac{\mu v}{W}$$

The value of the right hand bracket may be estimated similarly for the same point:

$$\left(\frac{rv\rho'}{\rho}\right) + \left(\frac{rv\rho'}{\rho}\right)' \ \eta = \epsilon$$

$$\left(\frac{rv\rho'}{\rho}\right) + \left(2\left[u+v\right] + \frac{rW}{\mu}\right)' \ \frac{\mu v}{W} = \epsilon$$

The derivatives on the left are all available from the computations. The value of ϵ should go to zero faster than v does. In practice however, it may not. If this is owing to computational instability then the computation should be rejected after ϵ has passed through a small minimum, thus establishing the band-width across which the series expansion is to be used. If on the other hand ϵ does not pass through zero or a small minimum for a given pair of values of k_3 and k_9, then these must be adjusted to give pairs of values for which ϵ does become small, this process

being essentially a restriction on the initial constants. Having arrived at values of η and r_o, a series expansion may be employed. Let:

$$v = (v)_o + (v)_1 \eta + \ldots$$

$$u = (u)_o + (u)_o \eta + \ldots \quad \text{etc.}$$

All quantities in ( ) are constant coefficients.

Substituting these in the set (4. 8) and letting $(v)_o = 0$, the coefficients of the first order (first derivatives) may be determined in terms of the zero order coefficients. The selection of both v and the right side of the first equation to be 0 at r_o is equivalent to two conditions; there are eight remaining zero order coefficients which can be independently picked, giving a total of ten conditions as before. The first order coefficients thus determined will be substantially the same as the first derivatives as computed from (4. 8) at the edge of the instability band, with the possible exception of the expression for $(\rho)_1$, which is given by the expression

$$(\rho)_1 = -\frac{(\rho)_o (\mu)_o}{(W)_o} \left\{ \frac{2}{r_o} \frac{(\omega)_o}{(\mu)_o} - \frac{6}{r_o^2} (u)_o + \frac{3}{4} \text{Re} \frac{(P_o)_1}{(\mu)_o} - \frac{(W)_o (\mu)_1}{(\mu_o)^2} \right\}$$

where

$$(P_o)_1 = \frac{\left\{ (\Gamma)_o (\rho)_o (\phi)_o + (\mu)_o (\Gamma)_o \cdot D \cdot (h_o)_o + (\mu)_o (\Gamma)_1 (\rho)_o (h_o)_o \right\}}{(\mu)_o \left\{ 1 - \frac{3}{8} r_o \cdot e \frac{(\Gamma)_o (\rho)_o (h_o)_o}{(u)_o (\mu)_o} \right\}}$$

$$(\Gamma)_o = \frac{1}{2} \frac{R_{air} + (R_{gas} - R_{air}) (C)_o}{C_{P_{air}} + (C_{P_{gas}} - C_{P_{air}}) (C)_o}$$

$$(\Gamma)_1 = \frac{1}{2} \frac{\left\{ -R_{air} (C_{P_{gas}} - C_{P_{air}}) + C_{P_{air}} (R_{gas} - R_{air}) \right\}}{\left\{ C_{P_{air}} + (C_{P_{gas}} - C_{P_{air}}) (C)_o \right\}^2} \frac{(x)_o}{(\mu)_o}$$

$$D = -\frac{(\rho)_o (\mu)_o}{(W)_o} \left\{ \frac{2}{r_o} \frac{(\omega)_o}{(\mu)_o} + \frac{2}{r_o} \cdot \frac{(W)_o}{(\mu)_o} - \frac{2(u)_o}{r_o^2} - \frac{(W)_o (\mu)_1}{(\mu)_o^2} \right\}$$

$$(\mu)_1 = \frac{1}{2} \frac{(\mu)_o}{(h_o)_o} \left\{ \frac{(\phi)_o}{(\mu)_o} - (\mu)_o^2 \left[\frac{2 C_{P_{gas}} T_\infty}{V_\infty^2} - \frac{2}{M^2 (\gamma_{air} - 1)} \right] \frac{(x)_o}{(\mu)_o} \right\}$$

This formula for $(\rho)_1$ is non-singular and is given in terms of the zero order coefficients at the stagnation point. If, however the values of u, ρ etc., are used from machine results at the outer edge of the instability band, then (for small η) the error committed will be of higher order than the approximations given here. Thus a stable value of $d\rho/dr$ is obtained which is consistent with the conditions at stagnation. Of course the values of the quantities (u, p ---) and their first derivatives may now be used for a linear extrapolation across the instability band to re-establish the machine computations with correct values of the dependent variables. The integration may continue to the inner flow and be matched as described in the next section. For completeness the remaining relations are given here for the series solutions at stagnation:

$$(W)_0 \text{ must } = -2(u)_0(\mu)_0/r_0$$

$$\text{for } (v)_0 = 0$$

$$(v)_1 = (W)_0/(\mu)_0 \qquad (u)_1 = (\omega)_0/(\mu)_0$$

$$(W)_1 = (3/4)\text{Re} \cdot (p_0)_1$$

$$(\omega)_1 = \left(\text{Re}/r_0\right)\left\{(\rho)_0(u)_0^2 + 2(p_2)_0 - 2(p_0)_0\right\}$$

$$(C)_1 = (x)_0/(\mu)_0 \qquad (p_2)_1 = (\rho)_0(u)_0^2/r_0$$

$$(h_0)_1 = (\phi)_0/(\mu)_0 \qquad (H_0)_1 = (\phi)_0/(\mu)_0$$

$$(\phi)_1 = 0 \qquad (x)_1 = 0$$

The algebraic relations give:

$$(P_0)_0 = (\Gamma)_0(\rho)_0(h_0)_0$$

$$(h_0)_0 = (H_0)_0$$

$$(\mu)_0 = \left\{ \frac{(h_0)_0}{(C)_0 \cdot \dfrac{2C_{P_{gas}} T_\infty}{V_\infty^2} + \left[1 - (C)_0\right] \cdot \dfrac{2}{M_\infty^2 (\gamma_{air} - 1)}} \right\}^{\frac{1}{2}}$$

MC 63-80-R1

4.3.4 Matching Solutions With the Inner Flow

The discussion of inner boundary conditions in section 4.2.4 shows that when inviscid flow is reached, the equations will automatically require the zero order enthalpy H_0 to be a constant (H_G); similarly the value of C will become constant. The value of H_G can be fixed a priori by proper choice of k_1, as given by formula (4-11). According to (4.7), then, there remain two disposable properties of the inner flow: the value of C and of S_G. This is the same number as the number of available constants in the asymptotic solution at the outer edge (i.e. k_3 and k_9). Thus it will be possible to match the desired values C and S_G at the inner boundary.

The value of C must of course be one in all cases. The value of S_G, which is the entropy of the source flow, is a matter of choice. Since the inner flow is isentropic it is useful to keep a running check on the entropy (S), as given by

$$e^{S/R} = \frac{(h_o)^{\frac{1}{\gamma_G - 1}}}{\rho} \tag{4.20}$$

and the total energy H_o. When these have become nearly constant in the process of computation, the inner boundary has been reached. Denoting the final value of entropy by S_G, it can be seen that it is equivalent to a statement of the chamber pressure of the source flow, since from (4.20) and the equation of state, and using the fact that $h_o = H_G$ at source stagnation, one has:

$$e^{S_G/R_G} = \left(\frac{\gamma_G - 1}{2\gamma_G}\right) \cdot \frac{H_G^{\left(\frac{\gamma_G}{\gamma_G - 1}\right)}}{p_{G,\,chamber}}$$

There now arises the question of what kinds of inner source flows the solutions are capable of representing. It has been noted that the necessity of integrating through the dividing streamline (stagnation) may place restrictions on the choice of values for k_3 and k_9. In this regard it can be expected that if the asymptotic formulas (4.19) are correct, then any choice of k_3, k_8 and k_9 will yield a flow that is regular at stagnation (i.e. that any singular behavior there is merely computational instability). This would leave full freedom to match conditions on C and S_G. The other quantities however, such as u, v, ρ, H, and S, cannot be specified, but must be accepted as determined by the process of integration. It can be shown for example that if the inner flow is to have the same entropy along streamlines off the axis (i.e. $\phi \neq 0$), then p_2 must equal p_0; however there are not enough constants to enforce this condition. As a practical matter this lack is related to the inconsistency in some of the second order relationships as discussed in the previous annual report (ref. Hill and Habert (1963)). The details of the inner flow will have to await the completion of a number of solutions of the type discussed here.

MC 63-80-R1

4.4 Results of Numerical Analysis

As noted in 4.1, preliminary results have been obtained using an earlier method of calculation. Essentially this was to integrate from both sides of the merged layer using estimated properties of the solutions as boundary conditions and then to attempt to match flow properties at the center (singular point) by adjusting the boundary values. The final answer is obtained by applying successive corrections to the eight undertermined gradients and the value of the radius at the inside boundary. To that end, it is assumed that the value of any characteristic quantity, obtained when the integration is stopped at the singularity point, is a linear function of the corresponding initial parameters with which the integration has been carried out. These parameters consist of the four physically undertermined gradients at the outer edge, the corresponding four gradients and the initial value of the independent variable r at the inner edge. At the singular point, the values of any characteristic quantity obtained by integration from outside and inside is different. This difference is a linear function of the nine parameters mentioned above. The new values of the parameters are obtained by computing the increment which must be added to each in order that the difference be zero. Since there are nine parameters, a zero difference can be imposed on nine characteristic quantities. The latter computation is carried out by inverting a 9×9 matrix. The computation is repeated until the differences fall below a small given number. This scheme is sometimes referred to as the method of influence coefficients.

It is assumed that at an altitude of approximately 180 kilometers a missile is flying at 4 kilometers per second. The Mach number is 6.5 and the Reynolds number is 65. The pressure in the combustion chamber of the rocket is 46.4 atmospheres; its temperature is $3600°K$. The exhaust gases have a ratio of specific heat of 1.25, their molecular weight is 22. The result of the computation is presented on Figs. 4.2 and 4.3. The influence coefficients scheme has been arranged in order that the following characteristic quantities should match at the singular point:

$$\rho, \ v, \ u, \ c, \ h, \ \mu h', \ \mu c', \ \mu v', \ \mu u'$$

The total enthalpy matches by definition; the pressure term p_0 matches too because

$$p_0 = \Gamma(c) \, \rho h$$

The second order term p_2 has not been required to match. It is remarkable that the density, velocity components, enthalpy, and concentration match with an approximation of $3/1000$ or smaller and the gradient with an approximation of 3 per cent or smaller.
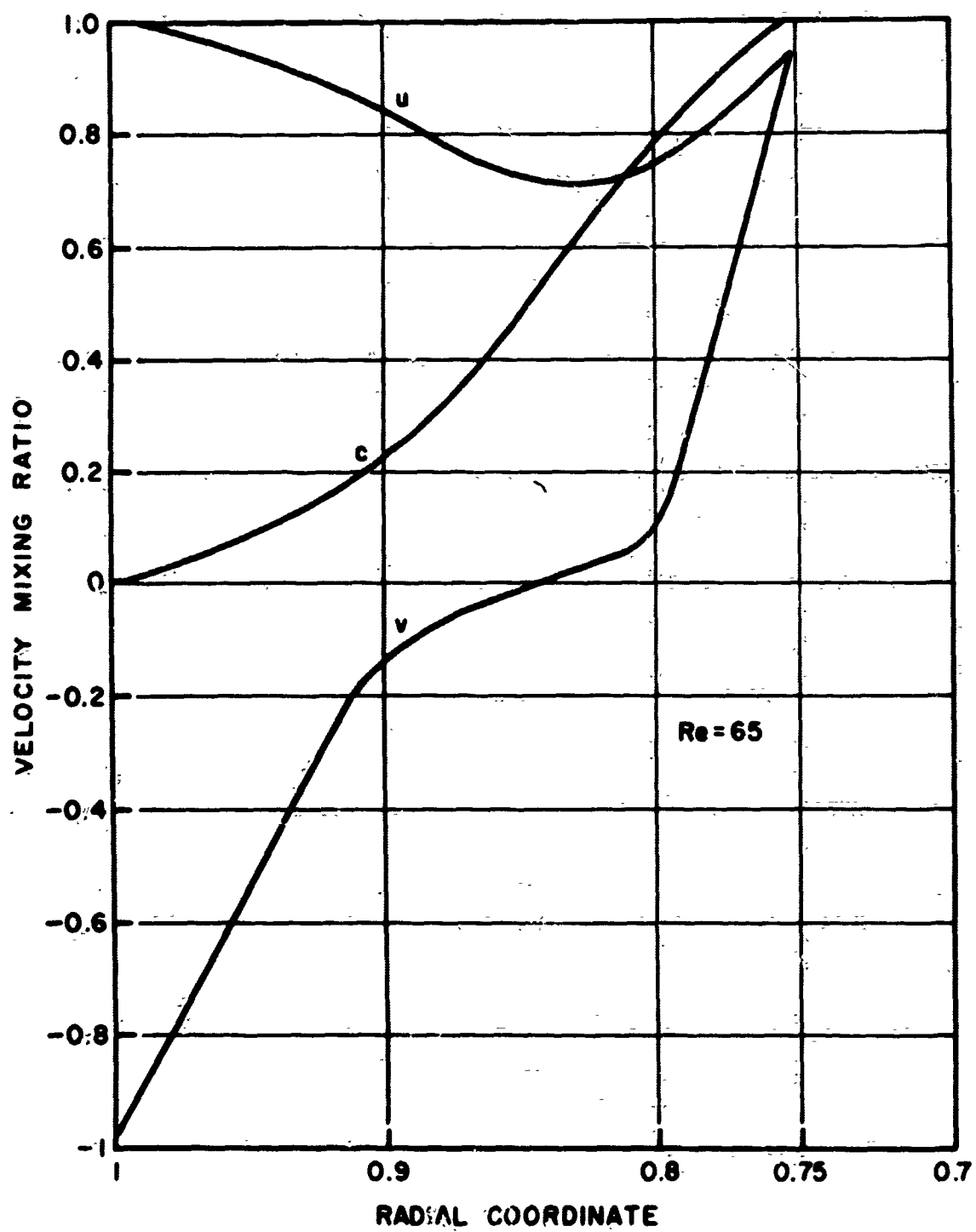
MC 63-80-R1

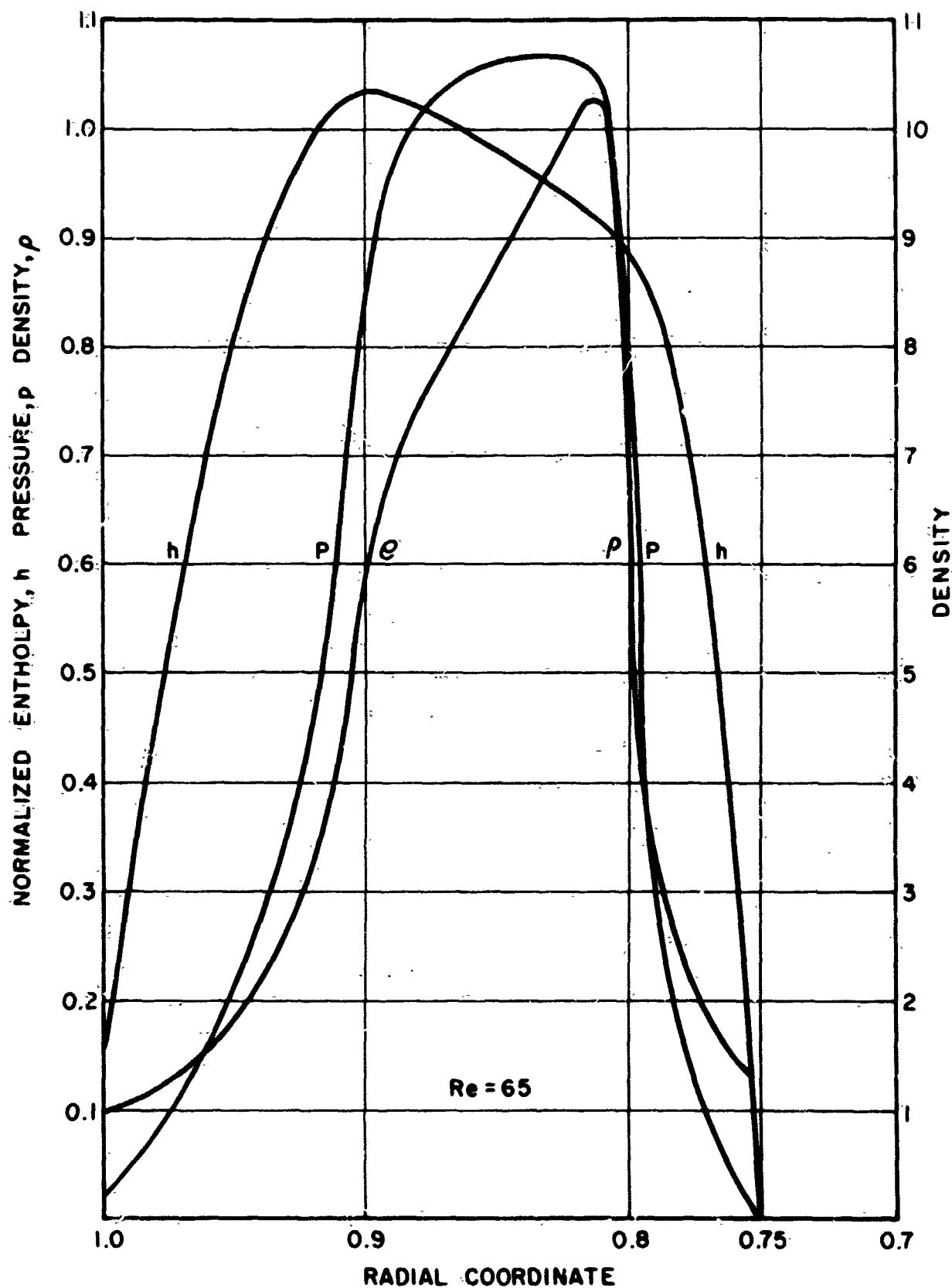Figure 4. 2. Stagnation Point Merged Layer Profiles

MC 63-80-R1

Figure 4. 3.   Stagnation Point Merged Layer Profiles

59   MC 63-80-R1

The sandwich-type structure of the merged layer is clearly illustrated by the results shown. There is a thick outer shock, $0.9 < r < 1.0$ approximately, in which the thermodynamic variables p, ρ and h rise to values very nearly equal to those for a thin shock in air at $M = 6.5$. There is an inner shock about half as thick, $0.75 < r < 0.80$, in which the exhaust gases are compressed. Here also the degree of compression is very nearly that which would be computed from the Rankine-Hugoniot equations. The inner shock is thinner because the temperature and hence viscosity of the gas approaching it is very much lower than that of the free stream. Between these two shocks is a layer across which the pressure is nearly constant. This corresponds to the mixing layer in the high-Reynolds number flow. The "dividing streamline," $v = 0$, is contained in this layer and the gradient of v is very much smaller than in the shocks. At this Reynolds number, however, the mixing extends beyond this region into the shock waves and the variation of mixing ratio in the constant-pressure region is only about $0.2 < c < 0.9$.

The structure of the merged layer at the nose of a high-altitude rocket plume is now known for one particular flight condition. It is well enough understood that qualitative extrapolation to both higher and lower altitudes is possible.

We recommend that additional and numerical integration of the equations be carried out to cover the range $5 < Re < 1000$. We would then be in position to continue the solution away from the stagnation point using approximate methods. The inner boundary conditions would be given by the analysis of Section 3.

The ultimate objective of this analysis is, of course, the prediction of the observables generated by the chemical reactions between the exhaust gases and the ambient. Work on this can be started immediately for those reactions for which the chemical kinetics have been established.

4.5 List of Symbols Used in Section 4

c	mixing ratio
$C_{P_{air}}$	specific heat at constant pressure for air
$C_{P_{gas}}$	specific heat at constant pressure for exhaust gases
$\mathcal{D}$	diffusion coefficient
h	specific enthalpy
H	total enthalpy
P_o, P_2	pressure terms
r	radial coordinate
R	radius of the outside sphere (see Fig. 4.1)
Re	Reynolds number based on the radius of the outside sphere and upstream conditions
R_{air}	perfect gas constant for air
R_{gas}	perfect gas constant for exhaust gases
R_{per}	perfect gas constant for any gas
S	entropy
S_{gas}	entropy of exhaust gases
u	tangential component of velocity
v	radial component of velocity
ν	specific volume
γ	ratio of specific heat
γ_{gas}	ratio of specific heat for exhaust gases
Γ	gas constant for the mixture of gases
θ	angular coordinate
μ	viscosity coefficient
∇	
M	

5. SHOCK WAVE FORMATION BY HIGH-ALTITUDE ROCKET PLUMES

5.1 General

The shockwaves generated by a rocket-powered missile in high-altitude flight are associated with the plume rather than with the body of the missile. As far as generating a disturbance in the ambient is concerned, the rocket plume acts just like a blunt-nosed body. Its size becomes very large at high altitudes; typical diameters at an altitude of 200 Km are several kilometers. Even though the ambient mean free path at these altitudes is very large by laboratory standards, it is still a small fraction of the plume diameter, so that continuum models of the flow may be used, and the formation of a shock wave is assured.

As the altitude and the size of the mean free path increase, the plume size increases also, for a given rocket motor burning at a constant rate. The simple blast-wave theory of Hill and Habert (1963) predicts, however, that the plume does not grow as fast as the mean free path, so that eventually a free-molecule model of the flow will have to be used and no shock wave will form.

The purpose of the work reported here is the development of an approximate criterion for the upper limit, in altitude, of shock wave formation. It is generally agreed that this limit occurs in the transition regime between continuum and free molecule flows. This regime is the most difficult one to handle theoretically and as Talbot (1962) has pointed out, there exists no really satisfactory theoretical prediction for the limit of formation of a well defined shock wave.

5.2 High Altitude Flow Regimes

Figure 5.1 copied from Levinsky and Yoshihara, (1961) illustrates schematically the flow regimes encountered by a re-entering hypervelocity 2-foot diameter sphere. The same range of flow regimes is encountered, in reverse order, by an ascending rocket-powered missile. The altitude for each regime is, of course, much higher in the latter case, because the plume is much larger.
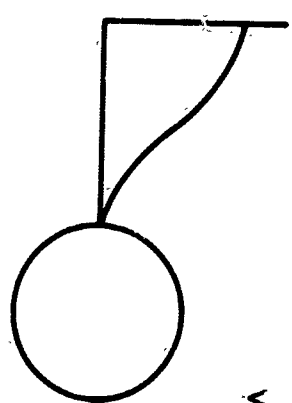
For the three flow regimes in the lower row of the figure, continuum theory applies and a shock wave is formed. Note that the
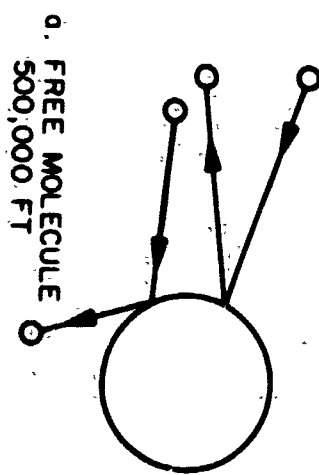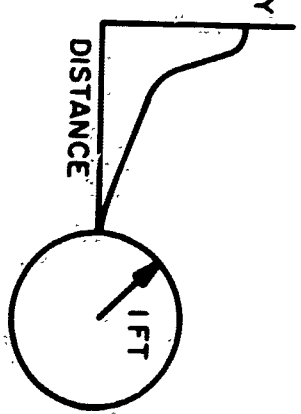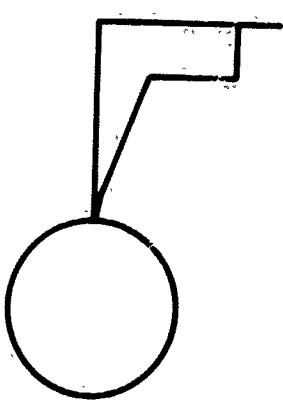
a. FREE MOLECULE
500,000 FT
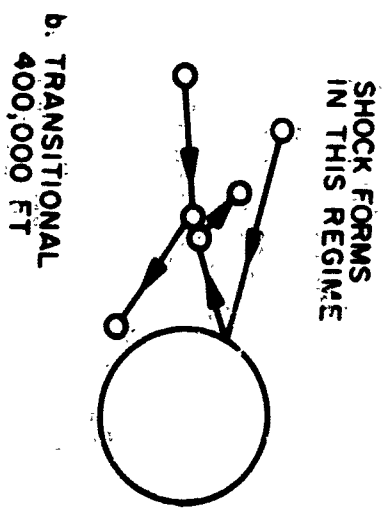
b. TRANSITIONAL
400,000 FT

SHOCK FORMS
IN THIS REGIME

c. FULLY MERGED LAYER
M=10, Re=100
300,000 FT

LIMIT OF SHOCK WAVE THICKNESS CALCULATION

d. INCIPIENT MERGED LAYER
M=10, Re=1000
250,000 FT

VELOCITY

DISTANCE

1 FT

e. BOUNDARY LAYER
M=10, Re=10,000
200,000 FT

Figure 5.1. Flow Regimes in High-Altitude Hypersonic Flight (after Levinsky and Yoshihara-1961).

shock thickness increases with increasing altitude and decreasing Reynolds number. The boundary layer thickness also increases and in the highest-altitude continuum flow regime the shock wave and boundary layer merge to gorm a single viscous layer between the body surface and the free stream. Hill and Habert (1963) have discussed the corresponding regime in the plume flow where two shocks and a mixing layer merge at the boundary between the ambient and the exhaust gases.

Consider now the flow in the limit of extremely high altitudes. Here collisions of air molecules with other air molecules are much rarer than collisions between the air molecules and the body and may be neglected in calculation of the flow pattern. This constitutes the "free molecular" regime of flight in which there is no pile up of molecules ahead of the body and no shock wave is formed. The corresponding regime in the plume flow is the "collisionless expansion" of exhaust gases.

In between the continuum and free-molecular flow regimes lies a transition regime in which collisions between air molecules cannot be altogether neglected. The molecules reflected from the body cannot penetrate indefinitely far upstream without colliding with other molecules in the ambient. As a result of such collisions there will be a tendency for molecules to pile up in front of the body and to form a region of increased density. The higher the ambient density, the smaller the penetration of the reflected molecules and thus the thinner the high-density region in front of the body. This is the process by which a shock-wave is initially formed as a body descends towards higher atmospheric densities. In the case of the plume flow the transitional regime corresponds to the onset of collisions between the ambient molecules and those from the rocket exhaust, forming a double shock containing a high-density region.

Figure 5.2 is a chart, again adressed to the re-entry problem, locating the various flow regimes around a 2-foot diameter sphere in altitude and velocity. Here Probstein (1961) has broken some of the regimes discussed above into sub-regimes which correspond to regions of validity of various mathematical approximations. Without much explanation he locates the limit of shock formation along the line where the shock thickness (estimated at 3 mean free paths) equals the body radius:

$$\delta_s \leq R_N \tag{5.1}$$

5.3 Criteria for Shock Wave Formation

Since there is a pile-up of molecules in front of a body even in free-molecule flow, it is difficult to establish a criterion for shockwave formation in terms of the density gradient there. It seems
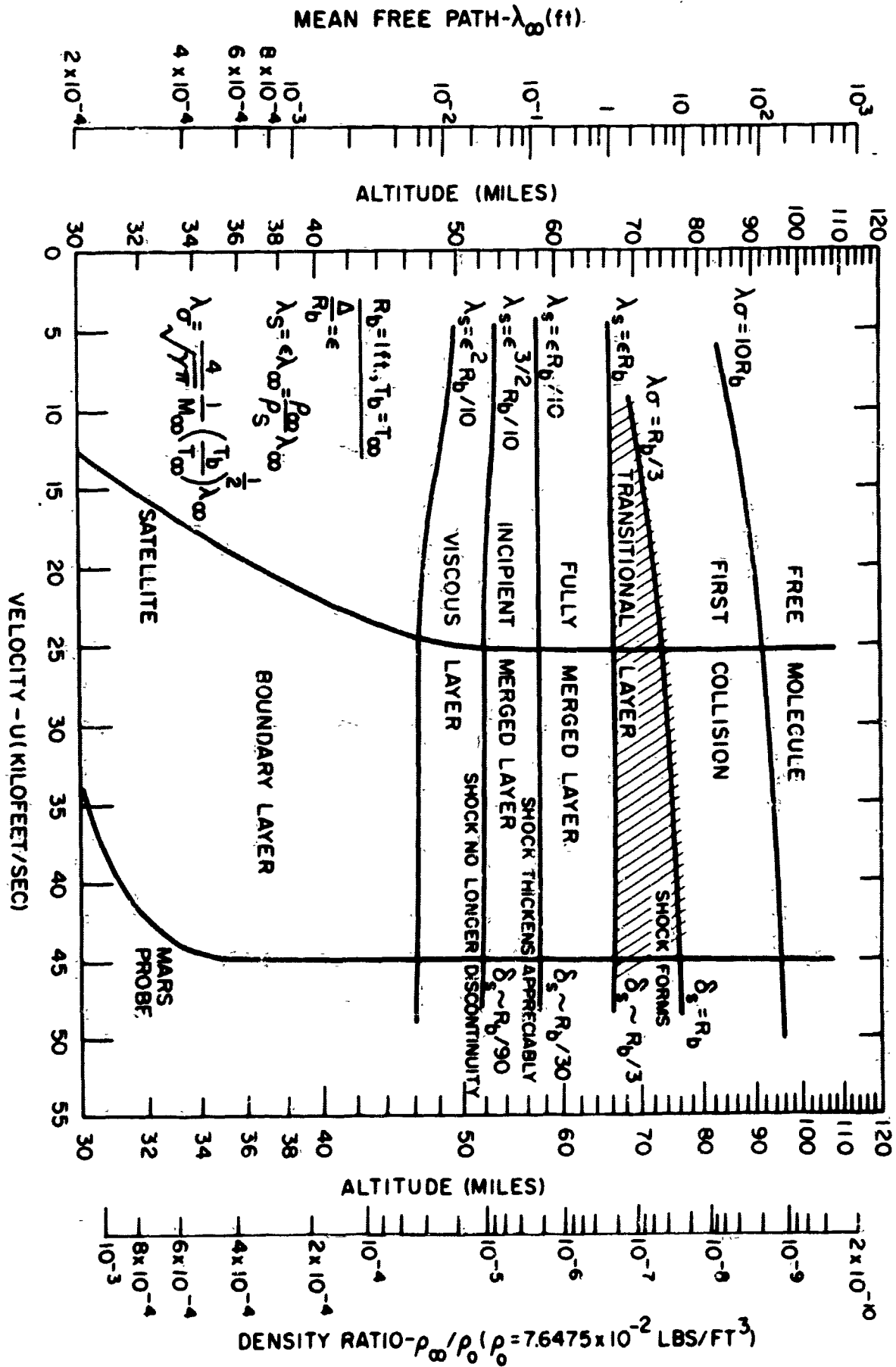
Figure 5.2. Flow Regimes for a 2-foot Diameter Sphere (after Probstein)

preferable to examine this question in terms of the lateral propagation of a density perturbation. Methods for calculating shock wave shape and decay at very low Reynolds numbers have been discussed by Lighthill (1956). Although a specific calculation procedure has not been set up for either the blunt-body or the plume problem, Lighthill's results can be used more or less directly to establish a criterion.

The relevant conclusion expressed in Lighthill's article is that "acoustic disturbances decay according to the power laws given by shock wave theory while their Reynolds number exceeds about 1, and according to the exponential laws given by attenuation theory when $\bar{R}$ is less than about 1. (The former decay laws are more rapid in the former range, the latter in the latter.)" This means that if $\bar{R} > 1$, the bow wave ahead of a body or plume will propagate laterally approximately as predicted by blast-wave theory, while if $\bar{R} < 1$, the disturbance will die out very rapidly around the sides of the body.

Now Lighthill's model of thick shock waves with viscous dissipation is based on Burger's equation and his Reynolds numbers, $\bar{R}$, are not directly comparable with ordinary Reynolds numbers based on shock wave thickness. It is convenient, therefore, to consider the complete N-wave, consisting of the bow shock, the rear shock, and the expansion between them. In this case the Reynolds number is simply related to the ratio of shock thickness to the length of the whole wave.

Figure 5.3 illustrates schematically the N-wave generated by a sphere in both a high-density and a low-density flow. In the latter the shock wave thickness is of the order of the sphere radius. For the shock wave spacing shown, this thickness corresponds to about one quarter of the total length of the N-wave and it may be deduced from Lighthill's calculated profile shapes that this corresponds to $R \approx 2$. Note, however, that this argument is only qualitative since the spacing between the bow and rear shocks has only been sketched approximately. What it does show is that Probstein's (1961) arbitrary criterion can be reformulated in terms of the initial Reynolds number of the N-wave generated by the plume or body and hence in terms of the lateral rate of decay of this wave. Note that the value of $\bar{R}$ in an axisymmetric flow decreases with increasing distance from the axis so that a wave which decays according to the blast-wave law initially may eventually reach a point where it begins to decay much faster.

Now although the shock wave forms in the transitional regime, estimates of its thickness can only be obtained as extrapolations from the merged layer regime, where calculations are possible. These calculations yield a thickness at the stagnation point and not out where the N-wave begins to form. Since the thickening of the shockwave between these two points cannot be calculated, we have chosen the somewhat conservative criterion

$$\delta_s \leq \frac{1}{2} R_N \tag{5.2}$$

ce

(a) HIGH DENSITY FLOW

LIGHTHILL'S REYNOLD
NUMBER ≈ 2
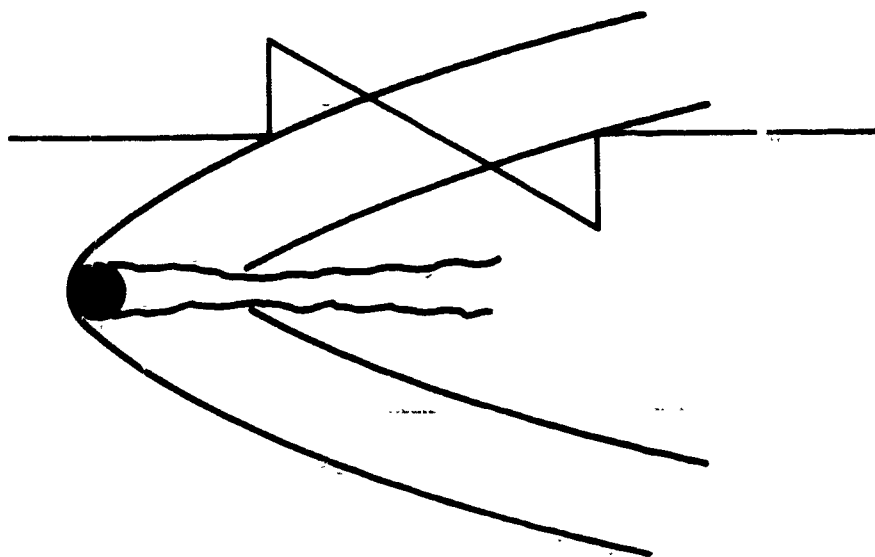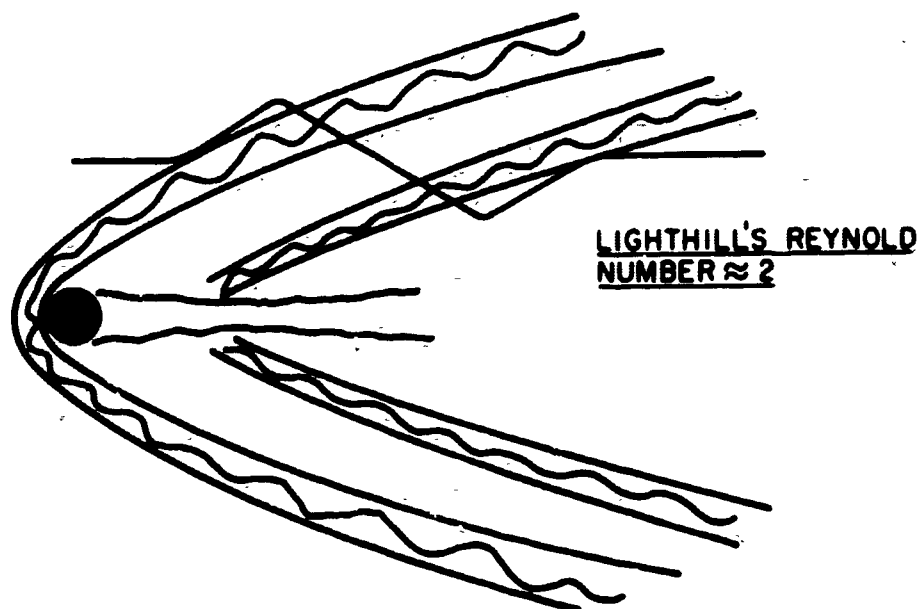
(b) LOW DENSITY FLOW

Figure 5.3.   Schematic N-Waves Generated by a
Hypersonic Sphere

which, starting from a completely different line of reasoning, only differs from Probstein by a factor of 2.

5.4 Estimates of Shock Wave Thickness

Extensive calculations (Liepmann et al (1962)) by means of the Boltzmann equation of the structure of plane shocks have shown that the Navier-Stokes model yields a good approximation to the thickness, if not to the details of the structure. We shall, therefore, estimate shock thickness in blunt-body and plume flows by extrapolating available Navier-Stokes calculations.

Figure 5.4 represents the results of numerical calculations of shock thickness in blunt-body flows. Three points have been taken from Kao's (1963) calculations of the flow past a sphere and one point represents our own initial calculation of the merged layer at the nose of a plume. The correlation parameter is

$$\frac{1}{M_\infty} \frac{\lambda_\infty}{R_N}$$

The inverse Mach number here accounts roughly for the variation between results obtained with different values of M_∞. It is consistent with the idea that shock thickness should depend on the mean free path behind the shock more strongly than on the one in the incident stream.

Extrapolation of these data to the critical value of Eq. 5.2 predicts the criterion

$$\frac{1}{M_\infty} \frac{\lambda_\infty}{R_N} \leq 0.4 \tag{5.3}$$

for the onset of shock formation.

The correlation parameter chosen here is essentially an inverse Reynolds number and it can easily be shown that (5.3) is equivalent to

$$Re = \frac{\rho_\infty U_\infty R_N}{\mu_\infty} \geq 4 \tag{5.4}$$

However the criterion in terms of the mean free path λ_∞ is easier to use since it is tabulated to higher altitudes.
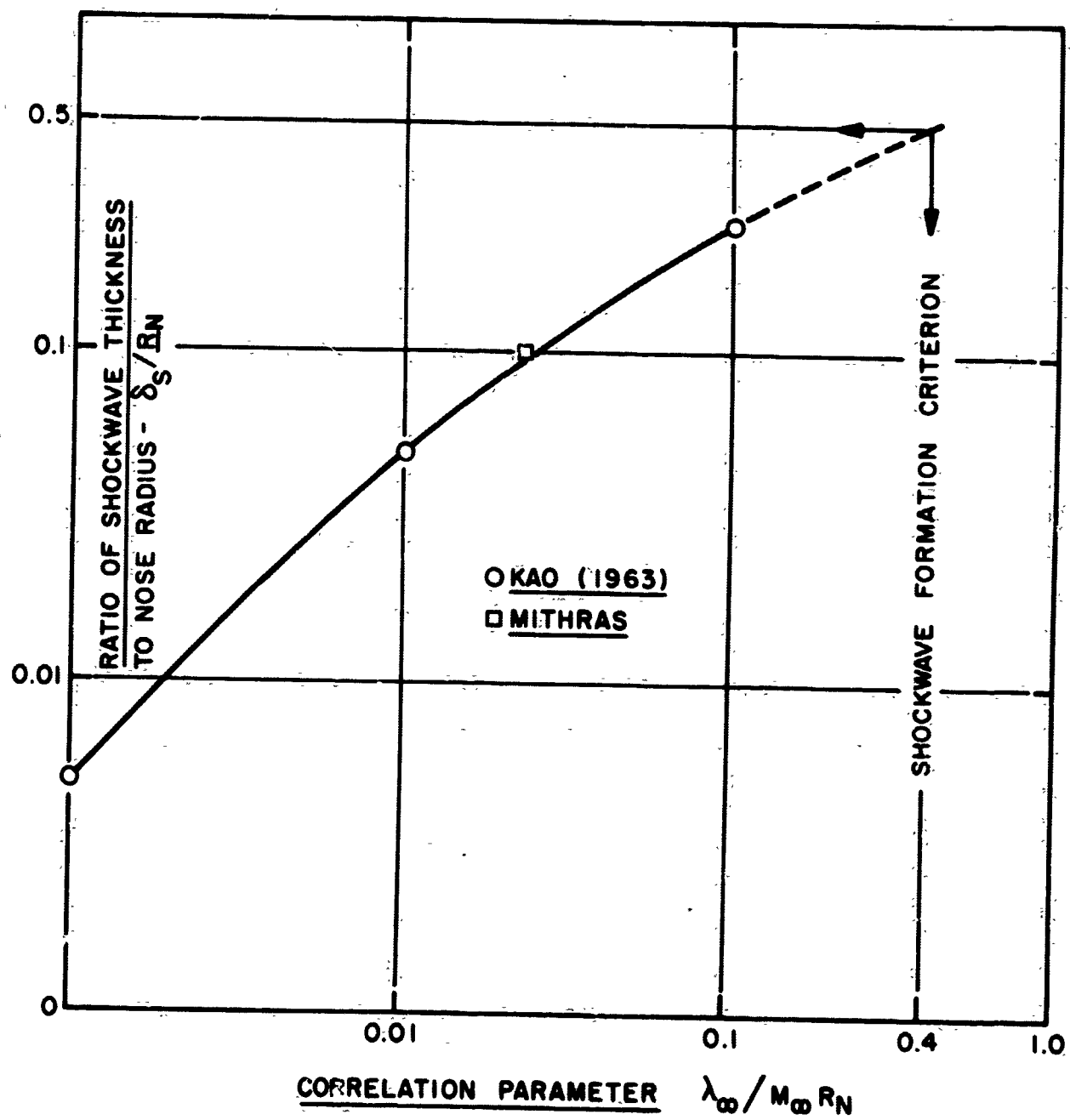
MC 63-80-R1

Figure 5.4. Shockwave Thickness in Merged-Layer Blunt-Body
Flows

69

5.5 Numerical Results

The nose-radius of a high-altitude rocket plume may be computed from the blast wave formula of Hill and Habert (1963)

$$R_N = \frac{0.4}{\sqrt{J_0}} \sqrt{\frac{\gamma_\infty D}{\rho_\infty V_\infty^2}}$$

$$= \frac{0.4}{M_\infty \sqrt{J_0}} \sqrt{\frac{D}{P_\infty}}$$

(5.5)

where D is the drag of the plume and J_0 is a parameter in the blast wave theory which depends on γ_∞. Over the range of γ_∞ of interest the constant value $J_0 = 0.85$ is a good enough approximation for the present purpose.

The validity of this theory in the transitional flow regime is, of course, dubious. Its prediction is nevertheless expected to be approximately correct. Neely (1964) has used it to estimate the plume size of the SYNCOM apogee motor at an altitude of 35,000 Km and found agreement to within half an order of magnitude with Baker-Nunn photographs.

The shock thickness correlation parameter may therefore be written

$$\frac{1}{M_\infty} \frac{\lambda_\infty}{R_N} \approx 2.3 \sqrt{\frac{P_\infty \lambda_\infty^2}{D}}$$

(5.6)

Figure 5.5 illustrates the variation of this parameter with altitude for two values of plume drag. Note that the plume drag value $D = 12,800$ lbs corresponds to the Atlas or Titan sustainer engine. Also shown in Fig. 5.5 is the limiting value of this parameter for shock wave formation, criterion (5.3). It predicts shock wave formation to very high altitude, above 400 Km for the Atlas and Titan engine.

The continuum-flow criterion used by Hill and Habert (1963) was

$$\frac{\lambda_\infty}{R_N} \leq \frac{1}{7}$$

This can be located in Fig. 5.5 only if a value of M_∞ is chosen. It has been drawn for $M_\infty = 6$, which is typical in the altitude range of interest. Note that it lies below the shock wave criterion by about
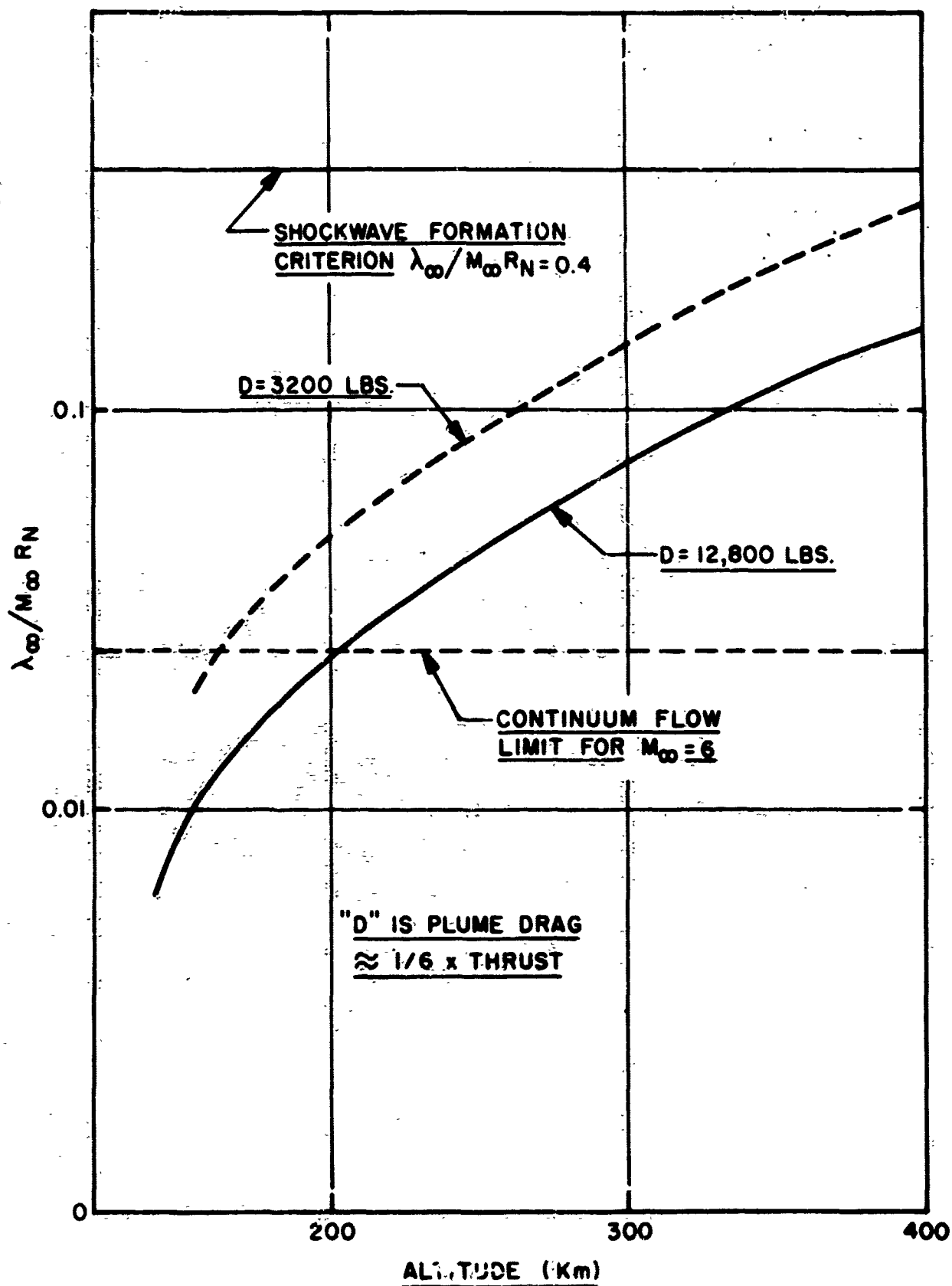
Figure 5.5. Shockwave Criterion Versus Altitude for Two
Rocket Plumes

MC 63-80-R1

one order of magnitude. According to Probstein's (1961) chart illus-
trated in Fig. 5.2, this spread is too large; a less severe criterion
for continuum flow would be more appropriate.

5.6 Conclusions

The development in this section of a criterion for shock wave
formation by high-altitude rocket plumes is based on estimates of
the Reynolds number of the N-wave formed by the bow and rear shocks
generated by the plume. The following conclusions may be drawn:

1. A more precise expression of the criterion developed
    will require a better model of the rear shock in a plume
    flow.

2. Given the length of the N-wave, the new criterion may
    easily be related to the more familiar criteria given in
    the literature in terms of the ratio of shock thickness
    to nose radius, δ_s/R_N.

3. Extrapolation of Navier-Stokes solutions for both sphere
    and plume flows has provided simple estimates of
    δ_s/R_N in terms of the parameter $\lambda_\infty/M_\infty R_N$ which is of
    the form of a reciprocal Reynolds number.

4. Using plume-size estimates given by blast-wave theory
    it has been shown that a shock wave will be formed
    throughout the burning period of typical ICBM engines.

MC 63-80-R1

REFERENCES

H. Alden (1963) Asymptotic Flows of Jets Exhausting to Vacua. MITHRAS Internal Memorandum No. 376A, February 3, 1963. (Unclassified)

H. Alden, R. Habert and J. Hill (1963) Gas Dynamics of High Altitude Rocket Plumes Semi-Annual Technical Report - MITHRAS, Inc. Cambridge - MC 63-80 ARPA Project Defender Order 42. (Unclassified)

J. Bowyer, Jr. (1958) Determination of the Envelopes and Lines of Constant Mach Number for an Axially Symmetric Free Jet Convair-Astronautics, San Diego. (Unclassified)

L. Goldberg and S. Scala (1962) Mass Transfer in the Hypersonic Low Reynolds Number Viscous Layer, Institute of the Aerospace Sciences Preprint 62-80. (Unclassified)

J. Hill and R. Habert (1963) Gas Dynamics of High Altitude Missile Trails, MITHRAS, Inc. Cambridge, Mass. MC 61-18-R1. Final Report Contract No. AF 19(628)-415. ARPA Order No. 42-61. ASTIA 415 111. (Unclassified)

H. Kao (1963) A Study of Viscous Hypersonic Flow Near the Stagnation Point of a Sphere. American Institute of Aeronautics and Astronautics Preprint 63-437. (Unclassified)

E. Levinsky and H. Yoshiara (1961) Rarefied Hypersonic Flow over a Sphere, American Rocket Society Preprint 1957-61. (Unclassified)

H. Liepmann, R. Harasimaha, and M. Cahine (1962) Structure of a Plume Shock Layer, The Physics of Fluids, (November 1962). (Unclassified)

M. Lighthill (1956) Viscosity Effect in Sound Waves of Finite Amplitude Surveys in Mechanics, G. I. Taylor 70th Anniversary Volume, Cambridge, University Press. (Unclassified)

H. Mirels, and J. Mullen (1962) Expansion of Gas Clouds and Hypersonic Jets Bounded by a Vacuum, Aerospace Corporation Report TDR-169 (3230-12), TR-1. (Unclassified)

G. Neely, (1964) Application of Blast-Wave Theory to Prediction of Plume Size for SYNCOM Apogee Motor (U), Semi-Annual Report of BAMIRAC, Institute of Science and Technology, University of Michigan (February 1964). (Secret)

REFERENCES (Cont)

R. Probstein (1961). Shock-Wave and Flow Field Development in Hypersonic Re-Entry, American Rocket Society Journal Volume 31, No. 2. (Unclassified)

N. Rosenberg, et al (1961) High Altitude Missile Train Dynamics (U) AMRAC Proc., Project Defender Meeting 15-17 November 1961; Vol V, Part 1. (Secret)

L. Talbot, (1962) Survey of the Shock Structure Problem (U) A. R. S. Journal (July 1962). (Unclassified)

H. Tsien, (1958) Fundamentals of Gas Dynamics, Edited by Howard W. Emmons; Vol. III of High Speed Aerodynamics and Jet Propulsion, pp 57-60; Princeton University Press. (Unclassified)

G. Witham, (1950) The Behavior of Supersonic Flow Past a Body of Revolution, Far from the Axis. Proc. Roy Soc A201 89. (Unclassified)

MITHRAS, Inc., Cambridge, Mass. MC 63-80-R1
GAS DYNAMICS OF HIGH-ALTITUDE ROCKET PLUMES by
H. L. Alden, et al. Air Force Cambridge Research
Laboratories, Bedford, Mass. Scientific Report Number
AFCRL-64-677, vi and 74 pages, July 1964.
Unclassified Report

This report describes methods for calculation of the
velocities and thermodynamic properties of flow fields
through and around high altitude rocket plumes. The main
effort is directed at obtaining a good representation of both
the jet flow from rocket motors and the shock-mixing
layers in the frontal regions; the calculation then proceeds
downstream using standard methods. The work may be
divided in three parts: the development of methods to cal-
culate the flow fields throughout plumes using the principles
of inviscid continuum mechanics; the study of the shock-
mixing layer structure at the nose of the plume using the
general Navier-Stokes equations (i.e., accounting for vis-
cosity, heat conduction and diffusion); and an estimate of
validity of continuum mechanics for describing high altitude
plumes, as inferred from a study of shock wave formation
at high altitudes. A comparison with available observations
shows good agreement with overall plume dimensions as
determined by the flow-field analysis. It may be concluded
that the analysis provides a sound gas-dynamic description
which may be used as a basis for investigation of the plasma
and chemi-electric properties of high altitude plumes.

1. Gas dynamics of high
   altitude rocket plumes.

2. Flow of jets into vacua.

3. Hypersonic flows near
   stagnation at low
   Reynolds number

I. Project No. 4984
   Task No. 498401
   ARPA No. 42

II. Contract
    AF19(628)-3280

III. H. L. Alden et al

IV. In DDC collection